Evaluation of variations of the frictional force between a bullet and a case in a loaded cartridge

Utvärdering av variationer av friktionskraften mellan en kula och en hylsa i en laddad patron

Mattias Hahlin

Faculty of Health, Science and Technology

Degree Project for Master of Science in Engineering, Mechanical Engineering

Credit Points 30 HP

Supervisor: Christer Burman

Examiner: Jens Bergström

Date: 03-08-2018

Abstract

To ensure that manufactured cartridges is safe to use, a tensile test is performed. The frictional force between the bullet and the case is required according to Normas standard to be between 15 – 75 Kg. Variations of the frictional force, with values outside of the standard had been noted by Norma Precision without understanding the cause. The aim of this report was to investigate and evaluate possible causes of the variations measured by tensile tests, difference between extreme values and to find a solution to what can be done to prevent the variations. Two different cases and three different bullets were used by request from Norma in the scope of this report. Different combinations of the bullets and cases was tested by alternating process parameter, surfaces and loading procedures. The loaded cartridges went through tensile tests to investigate differences. Bullets and cases with extreme values from the measured frictional force were chosen for further investigation in SEM and profilometer. To be able to draw further conclusions four different simulation models was created in Abaqus and different parameters was calculated. The dimensions and shape of the bullet resulted as the cause of changes of the tensile test curves. The smallest frictional force was found to differ from the largest by a change in wear mechanism from mainly abrasive ploughing to cutting and adhesion that caused transfer of material from the bullet to the case. The change in wear mechanism was found to be caused by an increased bullet diameter. The loading procedure was found to cause variations in plastic deformation on the neck of the case and damage the bottom of the bullet. The loading procedure was assumed to have the largest impact on the variations in frictional force. To minimize the variations the central axis of the case was suggested to be in line with the central axis of the bullet.

Sammanfattning

För att säkerställa att tillverkade patroner är säkra att användas, utförs ett dragprov. Friktionskraften mellan kulan och hylsan måste enligt Normas standard, vara mellan 15 och 75 kg. Variationer av friktionskraften, med värden utanför standarden, hade noterats av Norma Precision utan att förstå orsaken. Syftet med denna rapport var att undersöka och utvärdera möjliga orsaker till variationer av friktionskraften mätt genom dragprov, skillnaden mellan extrema värden och att hitta en lösning på vad som kan göras för att förhindra variationer. Två olika hylsor och tre olika kulor användes på begäran av Norma inom ramen för denna rapport. Olika kombinationer av kulor och hylsor testades genom att alternera processparameter, ytor och laddningen. De laddade patronerna gick igenom dragprov för att kvantifiera skillnader. Kulor och hylsor med extrema värden från de uppmätta friktionskrafterna valdes för vidare utredning i SEM och profilometer. För att kunna dra ytterligare slutsatser skapades fyra olika simuleringsmodeller i Abaqus och olika parametrar beräknades. Kulans dimensioner och form resulterade som orsak till ändringar av dragprovkurvorna. Den minsta friktionskraften upptäcktes skilja sig från den största genom en förändring av nötningsmekanismer från huvudsakligen abrasiv plogning till skärning och adhesion som även orsakade överföring av material från kulan till hylsan. Förändringen av nötnings mekanismer visade sig vara orsakad av en ökad diameter på kulan. Laddningen visade sig orsaka variationer i plastisk deformation av hylsans hals samt skada botten av kula. Lastningsproceduren ansågs ha störst effekt på variationerna i friktionskraften. För att minimera variationerna föreslogs att hylsans centrala axel ska vara i linje med kulans centrala axel.

Table of contents

1 Introduction

This master thesis is written by request from Norma Precision Ab. Norma Precision manufacture, test and develop cartridges for hunting and competitive shooting. They produce a great variety of cartridges with different materials, calibers, dimensions and shape. [1] For finished product they perform a quality control by tensile tests. This is made to ensure that the cartridge can be fired without causing large pressures inside the cartridge that can damage equipment and be dangerous for the user.

1.1 Cartridge

A cartridge contains of a bullet, case, primer and a gunpowder charge. When the firing pin of the rifle hit the primer the gun powder is ignited as seen in Figure (1). A pressure is built up inside the case until the frictional force between the bullet and the case is overcome and the bullet leaves the case and is accelerated through the barrel of the rifle. [1]

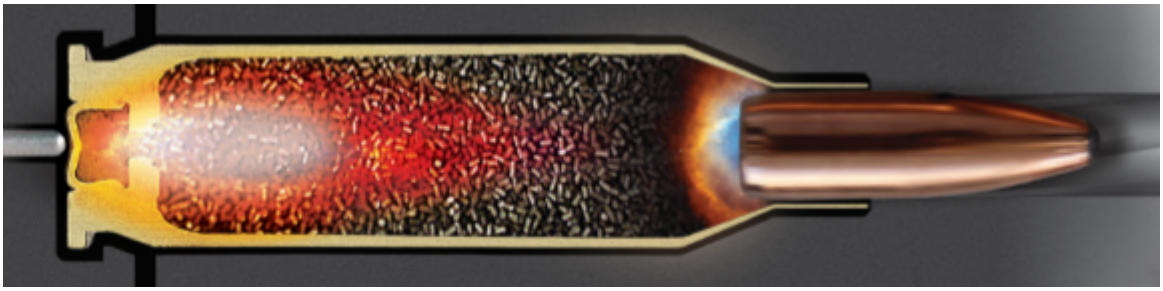

Figure 1: Loaded cartridge that is being fired. [1]

1.1.1 Cases

The cases investigated in this report by request from Norma are 300-Winchester-Magnum and 308-Winchester, seen in Figure (2) A and B respectively. The cases are manufactured in CuZn30 according to Ingemar Fogelberg (Manufacturing Engineering Manager) and Christian Gunnerbom (Quality manager) at Norma.

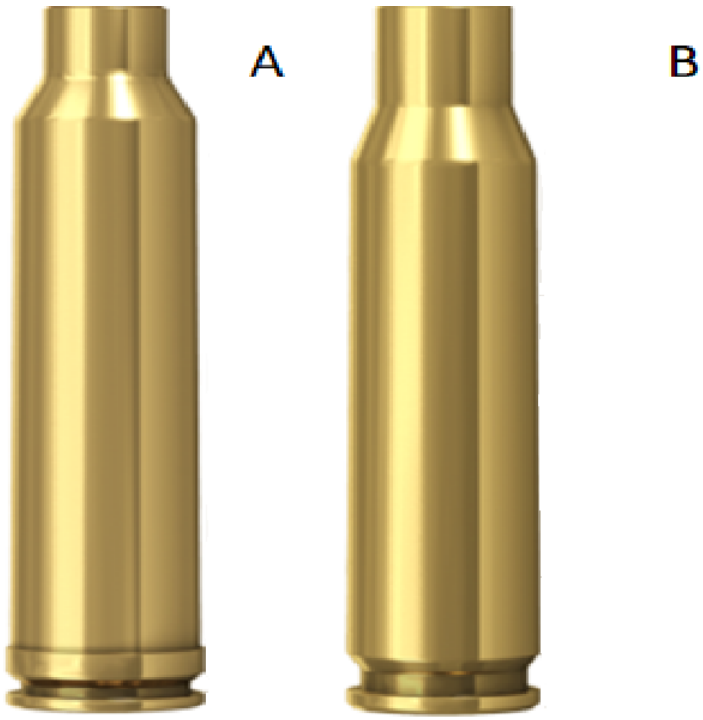

Figure 2: Cases used in the investigation, in A 300-Winchester magnum and in B 308-Winchester. [2], [3]

1.1.2 Bullets

The bullets are manufactured with a lead core inside a copper jacket seen in Figure (4) A. The bullets used by request from Norma are 30 Tip Strike (with and without cannelure) and Norma full metal jacket, seen in Figure (4) A and B respectively. A cannelure seen in Figure 3 A for these bullets is pressed after manufacturing to increase the diameter to create a larger frictional force. Both bullet jackets are manufactured in CuZn5.

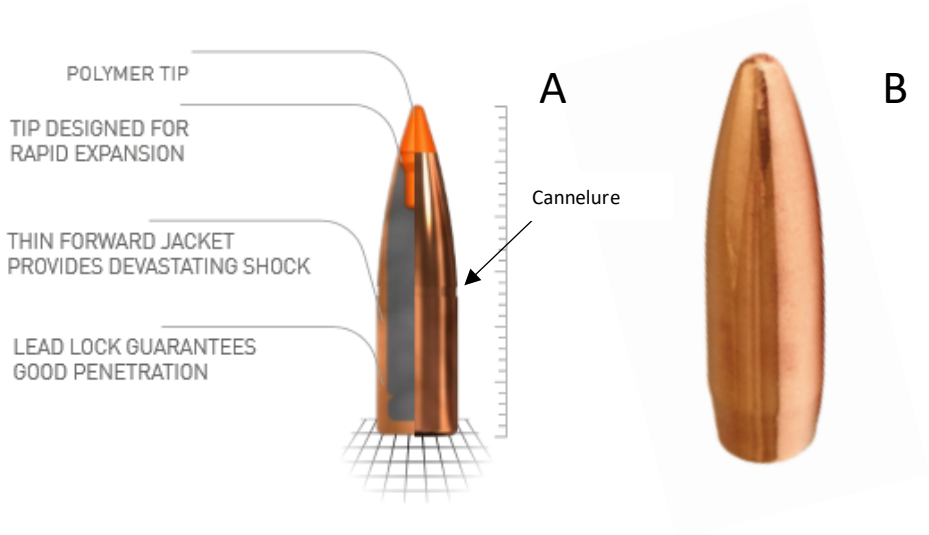

Figure 4: Bullets used in the investigation, in A 30 Tip Strike and in B Norma full metal jacket.[1], [4]

2 Aims and scope

Large variations of the frictional force have been discovered by Norma Precision during a quality control performed by tensile tests (described more in detail in Section 4.5). Manufactured cartridges are required to have a frictional force between 15 – 75 Kg to be safe to use. In the scope of this report parameters and processes that effects the frictional force is investigated and evaluated to give an answer to:

1. What is the main difference between cartridges with a large frictional force and a small?
2. Which processes, or parameter is the cause of these variations?
3. What can be done to prevent or minimize the variations in frictional force?

3 Theory

3.1 Friction

The friction force represents the resistance between two surfaces when applying a shear force and is described in Equation (1).

$$F = \mu W \tag{1}$$

Where μ is the coefficient of friction and W is the normal load.

The laws of friction states that:

1. The friction force is proportional to the normal load and
2. The friction force is independent of the apparent area of contact
3. The friction force is independent of the sliding velocity

3.1.1 Coefficient of friction

The coefficient of friction varies with sliding velocity, with the highest values for a static system. The static friction coefficient is influenced by the contact time, lubrication film properties, the elasticity of the tribological system, the mechanical properties of the materials, the contact pressure and the dissolution of materials. The static coefficient of friction for copper and brass is about 0,8 and 0,6 respectively. [5] The dynamic coefficient of friction varies with sliding velocity and load. For dry sliding with copper and brass, with a sliding velocity between 1-3 m/s and a normal load between 10-20 N, the coefficient has been determined between to be between 0,104 and 0,145. [6] For copper and copper alloys the surface layer is mainly responsible for the wear and frictional properties where large plastic deformation can be present after manufacturing. [7] The coefficient of friction includes both an adhesive term and a deformation/ploughing term as seen in Equation (2).

$$\mu = \mu_{def} + \mu_{adh} \tag{2}$$

The deformation component depends on shear strength and indentation hardness of the softer surface. The component can be calculated as seen in Equation (3) by assuming a conical asperity and that the indentation hardness is equal to the plastic flow stresses.

$$\mu_{def} = \frac{2}{\pi sin\alpha} \quad (3)$$

Where α is the angle of the spherical asperity.

The adhesive component of the friction coefficient

The adhesive component of friction is due to attractive forces between asperities in contact as seen in Figure (5) for adhesion without sliding and in the beginning of sliding. In the beginning of sliding in figure b plastic deformation by shearing of the softer surface is developed.

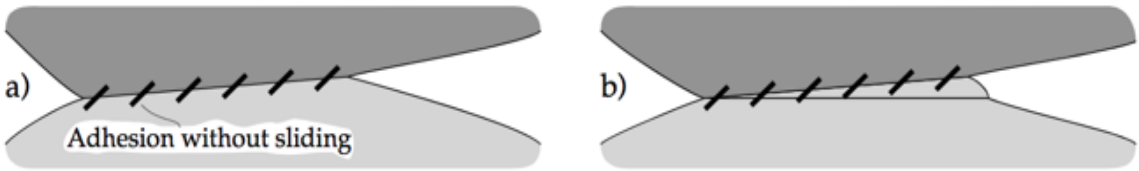

Figure 5: The difference between adhesion in a static in a) and a dynamic system in b). [8]

The adhesive forces can be large, sometimes larger than the normal force. The adhesive component of friction as seen in Equation (4) is controlled by the indentation hardness H and the shear strength S of the softer material. Evidence of adhesion can be seen by transfer of material from the softer surface to the harder one. Adhesion is prevented by an oxide layers on metals in contact. But with high loads and wear the layers can be penetrated by protruding asperities. [8]

$$\mu_{adh} = \frac{s}{H} \quad (4)$$

The largest values of the adhesive component are when two like metals are in contact. Because adhesion depend on many different parameters it gives a large uncertainty and variations in the frictional force. [9]

3.1.2 Junction growth

The real area of contact is determined by the asperity contacts. When a shear force is applied to two surfaces in contact this area can grow as seen in Figure (6), this is called junction growth. Because the coefficient of friction is direct related to the real area of contact a larger area will increase the frictional force. [8]

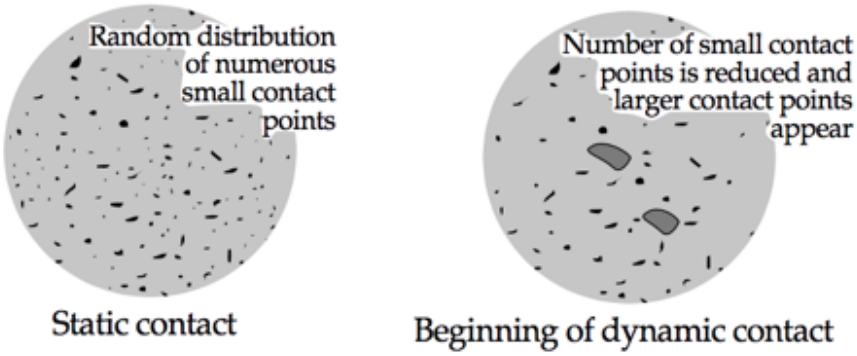

Figure 6: Difference in contact points between static contact and at junction growth at the beginning of dynamic contact. [8]

3.1.3 Surface Topography

The surface topography involves surface roughness which is small scale peaks and valleys on the surface, form error which is determined by measuring how much the shape deviate from the ideal shape (cylindrical, spherical or plane) and the waviness which is a periodic wave, which can be described by a wavelength and amplitude. The waviness and the surface roughness can be super positioned so that they create a surface profile Figure (7). [8]

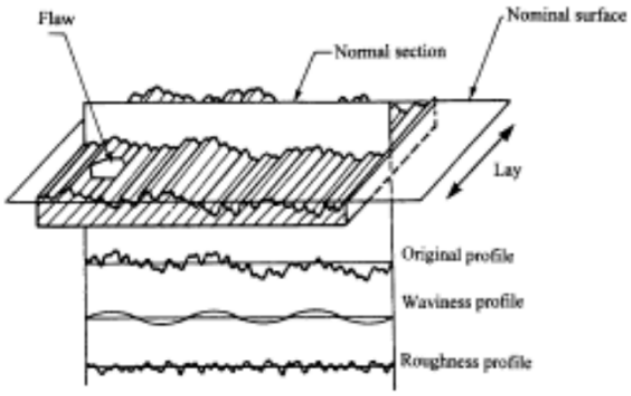

Figure 7: The surface topography separated into waviness and roughness. [10]

The most common way to describe the surface roughness in engineering purposes is by calculating the average surface roughness as in Equation (5).

$$R_a = \frac{1}{L}\int_0^L |z|\, dx \tag{5}$$

Where z is the height of the asperities along the length x divided by the total length L. Different surfaces with the same R_a value, can vary in frictional force due to different bearing of asperities on the surfaces. Surface roughness have an effect on both adhesion and wear by plastic deformation. Adhesion is reduced by increasing surface roughness or hardness of the contacting surfaces. But the asperities of a rough surface can wear by ploughing or groove formation on the softer surface of two contacting surfaces. [9]

3.1.4 Lubrication

Lubrication is used in manufacturing processes to decrease friction to avoid unnecessary wear of tools and damages on surfaces. In hydrodynamic lubrication the asperities of the counter facing surfaces are totally separated by the lubricating film. Boundary lubrication is due to molecules that are absorbed to the oxide layer of the metal. This limit and prevents junction growth and adhesion between the surfaces, which will decrease the coefficient of friction due to this easily, sheared layer. The molecular chains align perpendicular by adhering to the oxide layer with the polar end-groups. The molecules can carry most of the normal load by interactions.

The coefficient of friction is proportional to the size and length of the molecular chains of the lubricant. Long chains with a high number of carbon atoms will produce the lowest value of the friction coefficient. [8]

The most effective absorbing lubricants are fatty acids, but some organic compounds such as amides are also effective to reduce the coefficient of friction. [9] Different types of alcohols are also used for boundary lubrication and can give a very thin lubricating layer. [8]

3.2 Wear

Sliding wear occurs when two surfaces slide against each other. Sliding wear can be dry or lubricated. The main wear mechanisms for dry sliding is abrasion and adhesion.

3.2.1 Adhesive wear

Adhesive wear is severe wear mechanism that causes very high wear rates and can give large and unstable coefficients of friction or seizure. This can aggravate or prevent sliding motion as seen in Figure (5). The adhesive term of the frictional coefficient was earlier mentioned in Equation (4) dependent on both shear strength and indentation hardness of the two counter-facing surfaces. Adhesion can be suppressed by lubrication, increasing surface roughness and hardness of the surfaces in contact. Adhesion can vary of metals with similar hardness, this is believed to be caused how prone the material is to plastically deform by the asperities in contact that is a necessity to establish true contact. HCP metals have fewer slip systems than FCC metals why HCP metals are less prone to adhesion. Metals also can have an oxide layer that have to be penetrated to establish true contact. [9]

3.2.2 Abrasive wear

Abrasive wear is caused when particles deform or remove material from a counter-surface. The wear can be caused by two-body or three-body abrasive wear. In two-body abrasive wear material is removed or deformed by a protuberance in the counter-facing surface as in Figure (8) (a). Both hardness and surface roughness can affect the wear between the surfaces in contact. In three-body abrasive wear material is deformed or removed by particles between the counter-facing surfaces as in Figure (8) (b).

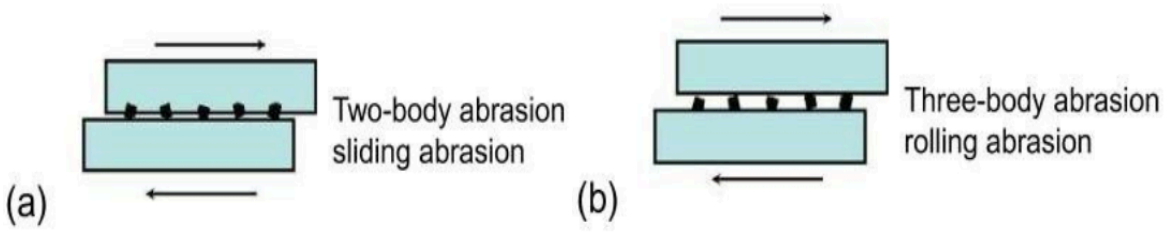

Figure 8: Abrasive wear by (a) two-body abrasion and (b) Three-body abrasion. [8]

The three main modes are mainly responsible for the wear is ploughing-, wedge formation- and cutting-mode. Removal of material due to plastic deformation is close related to the deformation component of the friction coefficient in Equation (3). In copper and brass large true strains can be introduced in the surface du to abrasion. This means that an increase in hardness in the bulk of the material will have a small effect due to the much higher strains introduced by abrasive wear particles. The frictional work due to abrasive wear is affected by the indentation and plastic deformation due to strain hardening in the surfaces in contact. [8]

3.3 Hardness

The hardness of metals is controlled by heat treatment, cold work and alloying. Heat treatment controls the grain size which as described in the next section controls the hardness as seen in Figure (9) due to a decrease in dislocation density and an increase in dislocations ability to move by decreasing the amount of grain boundaries. Cold work increases the dislocation density, twin density, shear bands and can create an anisotropic microstructure which affects the hardness and strength, as described in Section 3.4. [11] The hardness of copper and copper alloys can also be controlled by alloying. To increase the hardness silicon, iron, manganese and aluminum are used. [12] Cartridge cases are usually made from a single-phase brass alloy CuZn30, also known as α-brass which will be present up to about 32 % zinc at room temperature. Above 32 % zinc content a β-phase will be introduced. α-brass have a FCC crystal structure where zinc with a HCP crystal structure in solid-solution with the copper. Zinc creates good combination of ductility and strength which make them suitable for large amount of cold work. As seen in Table (1) a higher amount of zinc increases the strength but decreases the hardness. The bullet jackets where higher hardness is required to obtain its shape and wear resistance when used, have a small amount of zinc. [13]

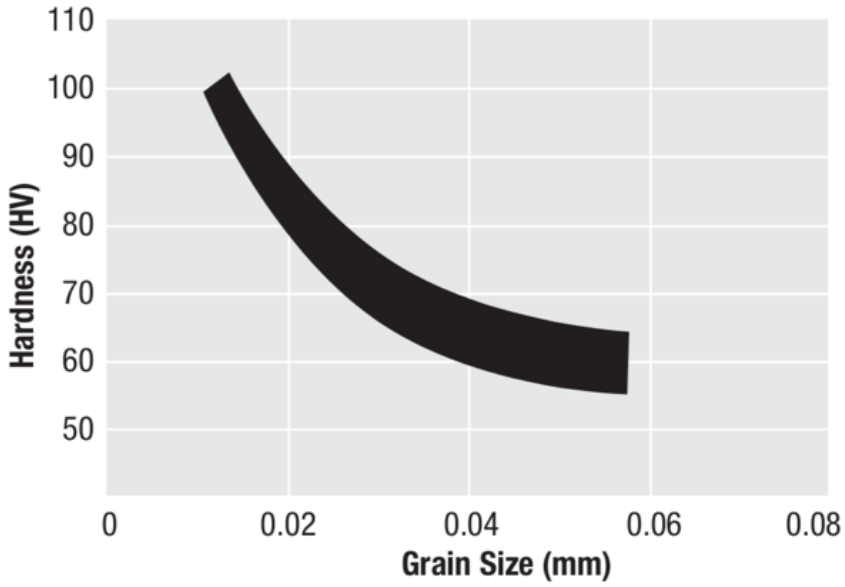

Figure 9: Hardness at different grain size for annealed CuZn30. [9]

3.3.1 Grain size effect

The grain size effect is the mechanical properties that are affected by a change in grain size. For large grains ductility increases and strength decreases. This can be explained by Equation (6), the Hall-Petch equation.

$$Y = Y_i + kd^{-1/2} \tag{6}$$

Where the yield strength Y is related to the basic yield stress or the stress that is required for the motion of dislocations, k is a constant which indicates to which extent dislocations are piled up at different barriers as twin and grain boundaries and d is the diameter of the grains. [11] The strength is related to the hardness of the material which therefore also related to the grain size.

This is true for except for grain size above a certain size. Then to large grain will decrease both ductility and strength. A coarse grain size during large plastic deformation can influence the surfaces negatively. Then the surfaces can roughen and develop a surface that can be resembled with orange peels as seen in Figure (10).

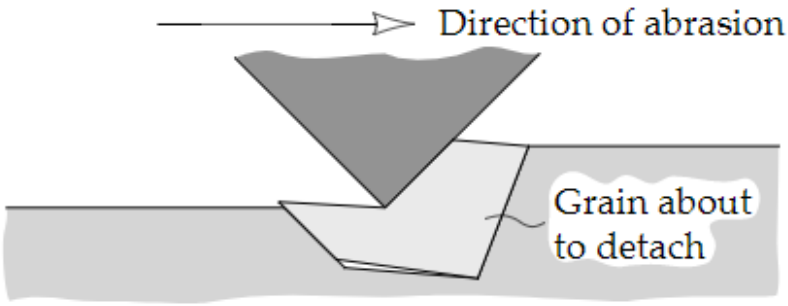

Figure 10: Effect of grain size on surfaces quality. [14]

A smaller grain size often gives better surfaces when the material is exerted to large plastic deformation. [13]

3.3.2 Hardening model

A common model to describe true stress above the yield point of a material is by the relationship seen in Equation (7) proposed by Hollomon.

$$\sigma_t = K\varepsilon_t{}^{\eta} \tag{7}$$

Where σ_t is the true stress, ε_t is the true strain, K is the strength coefficient (the true stress at ε_t=1) and η is the strain-hardening coefficient. The strain-hardening coefficient will in general increase with decreasing strength. [15]

3.4 Deep drawing

Cartridge cases and bullets are manufactured by deep drawing in several steps. During the process the raw material is pressed trough a die opening with a punch and extended along the sidewalls of the die. After the process the material will have a plastic anisotropy and be strained hardened. [16] To be able to continue deforming the material needs to be annealed to decrease dislocation density and tensile stresses. [14]

3.4.1 Deformation mechanisms

The amount of cold work is related to the mechanical properties of the material as seen in Figure (11). Tensile strength increases proportionally with the amount of cold work due to an increase in dislocation density, twinning and shear bands. For small deformation in low SFE metals the dominating deformation mechanism is dislocation slip. With further deformation twinning processes accompanies dislocation slip as deformation mechanism. For large deformations shear banding is the dominant mechanism.

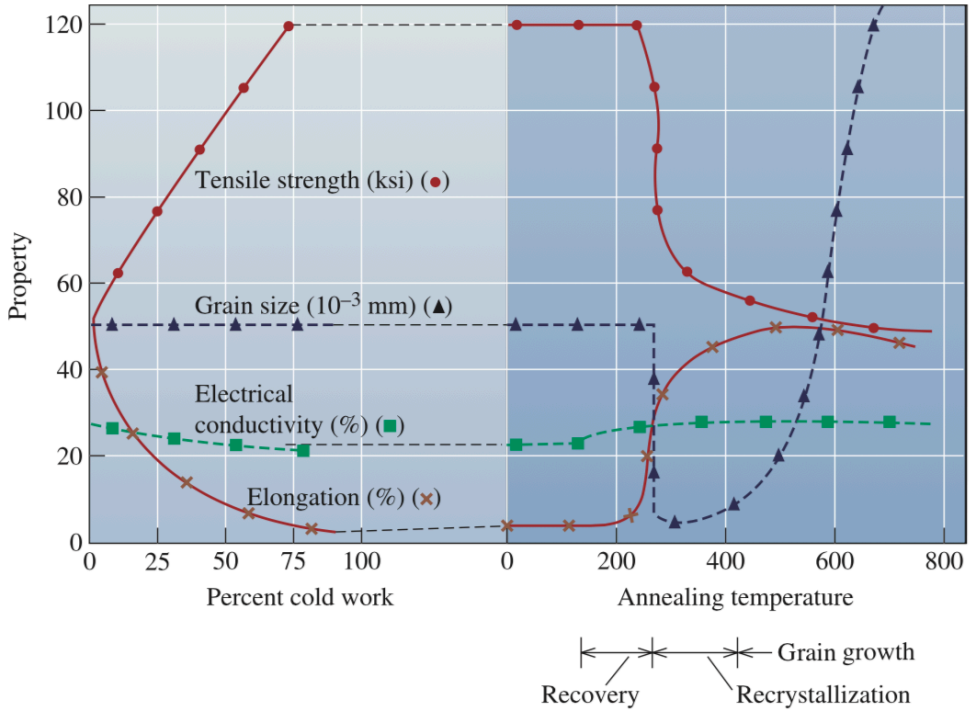

Figure 11: Tensile strength and grain size affected by different amount of cold work and annealing temperatures for CuZn35.

Dislocation slip

Dislocation slip is the dominant deformation mechanism for small deformation in copper and copper alloys. A dislocation is a line defect in the crystallographic plane of a material. A critical shear stress is needed to move the dislocations in a slip system. The critical shear stress is influenced by dislocation interactions, crystal structure and grain- and twin boundaries. With plastic deformation the dislocation density increases, and the material will be strain hardened.

Twinning

Twinning occurs because the absence of slip systems and difficulties for dislocations to move. Then the crystals lattice rotates and represents a mirror image of the other lattices across a twin boundary. Because of lower activation energy in low SFE in FCC crystal structures twinning is sometimes a preferred deformation mechanism then dislocation slip. Some researched have indicated that twin boundaries enhance strength by prevent dislocation movements as a grain boundary. [17] There are two types of twinning processes in materials, deformation twinning and annealing twinning. Deformation twinning is less common in FCC structure metals, because slip processes are more favored because of low SFE. [14] This mechanism is initiated at a critical dislocation density often at high strain rates. [18] Annealing twinning is common in some FCC alloys like brass. They are generated from preexisting plastic deformation and are created during recrystallization and growth of new grains. [14]

Shear band

For larger deformation, regions with very high dislocation density can be found known as shear bands. [19] They are a dominant mechanism to develop the microstructure in low SFE FCC crystals. They can be seen as narrow bands in the microstructure as in Figure (12) and

are increasing in density with increasing plastic deformation. [11] They are generated from inside of the twin-matrix layers and have a significant role in deformation, nucleation of recrystallized grains and the development of annealing textures. [19]. The deformation mechanism of asperities is usually by several shear bands of the softer or sharper one of two counter facing surfaces. A crack is initiated when the stresses over achieve a certain limit. [9]

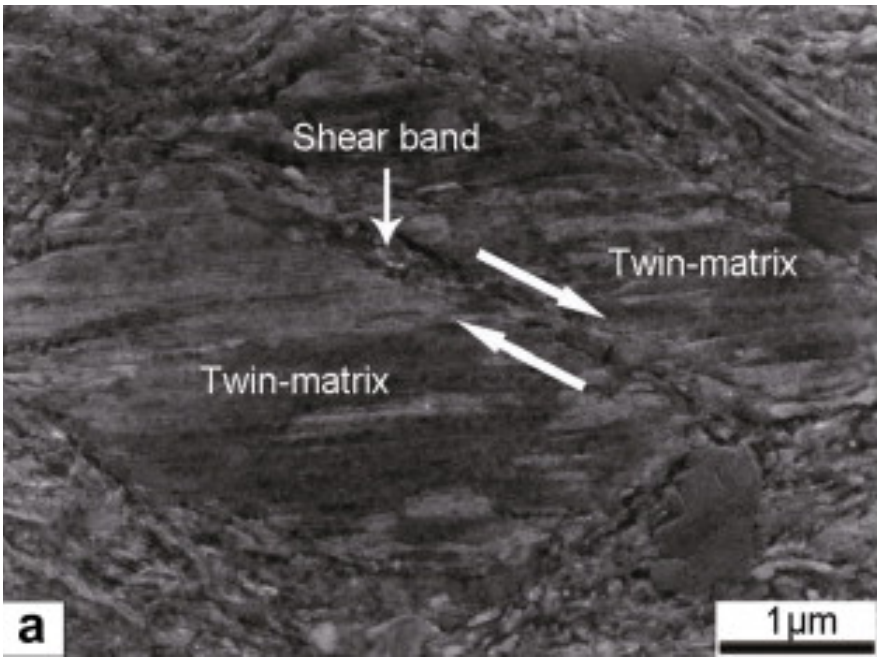

Figure 12: Shear band and twin matrix in alpha-brass after cold work with 98 % thickness reduction. [19]

3.4.2 Stacking fault energy (SFE)

The crystallographic planes are stacked in a certain order for different crystal structures. In FCC crystal structure the stacking sequence is ABCABC etc. A stacking fault happen when a surface defect causes an error in the normal sequence, which the planes in the crystal structure are stacked. Materials with low stacking fault energy such as brass have a high probability for stacking faults. SFE has a connection to the amount of strain hardening and the dislocation movements. Low SFE materials restricts cross slip by creating effective barriers that prevent dislocations to move. This means that low SFE materials will be strain hardened to a larger extent than high SFE materials. [14] SFE will influence the texture that will be developed during different amount of plastic deformation. This is because different deformation mechanisms will be dominant due to the crystal structure and stacking fault energy. [17] SFE is also related to the coefficient of friction. Materials with low SFE usually have larger coefficients of friction. [7]

3.4.3 Texture and anisotropy

When a metal is deformed the grains can be elongated and rotated in the direction which the stress is applied. This causes a crystallographic direction or texture which can give the material different properties in different directions. [11] The SFE will be responsible for which texture that will be developed depending on the magnitude of deformation, which is as described responsible for the active deformation mechanism. [17] Annealing will also affect the texture, there will be transitions between textures depending on the annealing time and temperature. [19]

3.5 Annealing

As seen in Figure (13) the hardness of brass is related to the annealing temperature, which as described in section 1.4.1 affects the strength. Annealing can be divided into three different stages. The first stage is recovery followed by recrystallization and grain growth. [20]

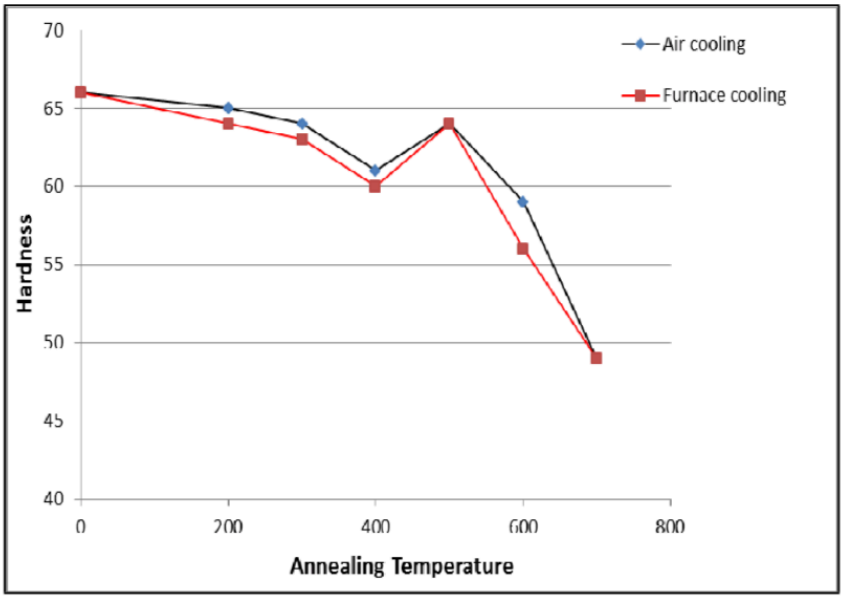

Figure 13: Hardness for different annealing temperatures for CuZn35. [20]

Recovery

After cold working the dislocation density increases and the material have residual stresses. A recovery anneal is made at low temperature to untangle dislocations in other words to reduce residual stresses, the dislocation density is basically unchanged during this treatment. [11] In Figure (13) the temperature for this treatment is between 150 – 250 °C for 30 – 60 minutes. [12] The hardness is decreased during this stage.

Recrystallization

The grain size is rapidly decreased during this stage because the growth of new small grains. This process requires a lower temperature if more cold work have been done on the material. [11] As seen in Figure (13) above 400 °C the hardness increases during this treatment. [20] Grain refinement is enhanced by mechanical twinning that suppresses dynamic recovery in cartridge brass. [21]

Grain growth

At higher temperature the grains start to grow to obtain a lower overall energy in the material. Grain growth is driven by the reduction of grain boundary area. [11] As seen in Figure (13) the hardness rapidly decreases during grain growth. [20]

3.5.1 Dezincification

During annealing of brass, the zinc content can be reduced due to evaporation called dezincification. Dezincification are a function of temperature and time as seen in Figure (14). This corrosion process leaves a porous metallic layer with high Cu content. [21] There are a great variety of results from research of dezincification. The reason is that it's a quite complex process with many different parameters that play a role in the process. [22]

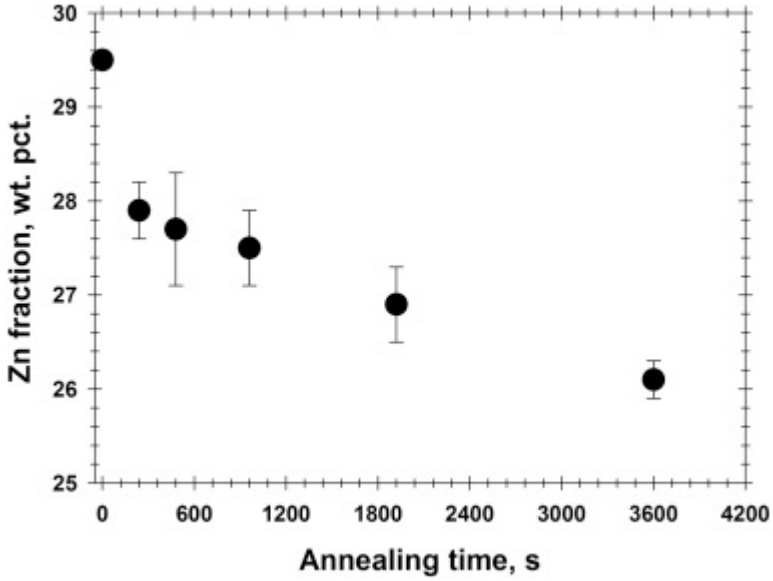

Figure 14: Dezincification of brass of different annealing times.

3.6 Surface treatment

Water is used in cleaning processes to carry residue material from manufacturing. An additive can be used to control the surface roughness. Sulfuric acid is used in a pickling process to remove the oxide layer on the surface. To stabilize the surface to avoid oxidation they can be passivated by using a passivation solution. [13]

3.6.1 Ideal gas law

The ideal gas law describes how the pressure in a gas changes with volume and temperature as seen in Equation (8). This shows the behavior of gases in conditions that is more perfect than in reality.

$$PV = nRT \tag{8}$$

Where P is pressure, V volume, n is the amount of substance in mole, R is the gas constant and T is the temperature. [23]

4 Method

4.1 Material

The cartridge cases are manufactured in CuZn30 and the bullets jacket is manufactured in CuZn5. The material data used simulations are showed in Table (1).

Table 1: Material parameters for CuZn30 and CuZn5. [15],[24]

Material	CuZn30 (C26000)	CuZn5 (C21000)
Hardness HV	68	115
σ_{Yield} [MPa]	115	95
Young's modulus [GPa]	105	120
Poissons's ratio	0,345	0,345
K	896	317
η	0,49	0,54

4.2 Manufacturing processes

In Table (2) the manufacturing processes for 300-Winchester-Magnum is written in order.

Table 2: Manufacturing processes for 300-Winchester-Magnum.

Manufacturing processes - 300-Winchester-Magnum
Annealing
Extrusion 1
Annealing
Extrusion 2
Annealing
Extrusion 3
Annealing
Extrusion 4
Cut neck to length
Shaping the base
Primer hole stamping
Annealing neck
Shaping neck
Calibrate neck
Punching magnum belt
Lath extractor groove
Degreasing
Annealing neck
Cleaning/pickling and Passivate

The manufacturing processes in yellow was assumed after discussion with Ingemar Fogelberg and Christian Gunnerbom to have the largest impact on the frictional force. This assumption

was made because the fourth extrusion step and neck calibration are the last processes that tools are in contact with the neck of the case. In these two steps the tools, both the punch and die were changed. The old tools had been used (according to responsible operator) for 300 000 – 400 000 cases. The cases with visual annealing were manufactured earlier, why no information of material origin or the wear of tools were available.

The bullet jacket seen in Figure (4) of both bullets used are manufactured through several extrusion steps by deep drawing. A lead core is then inserted inside the jacket and the tip is pressed. None of the bullets were produced during the tests, so no parameters could be controlled during the manufacturing processes, why no further investigation was made of the bullets manufacturing processes.

4.3 Measurements

All bullets and cases where numbered in each series. On the cases the inner diameter d_{Case}, outer diameter D_{case} and the concentricity C were measured before and after the tensile tests 1 - 10 with a Leitz PMM seen in figure (15) A. The measurements before the tensile tests are referred to 1 and after 2 (for example $d1_{Case}$ is the inner diameter before the tensile test).

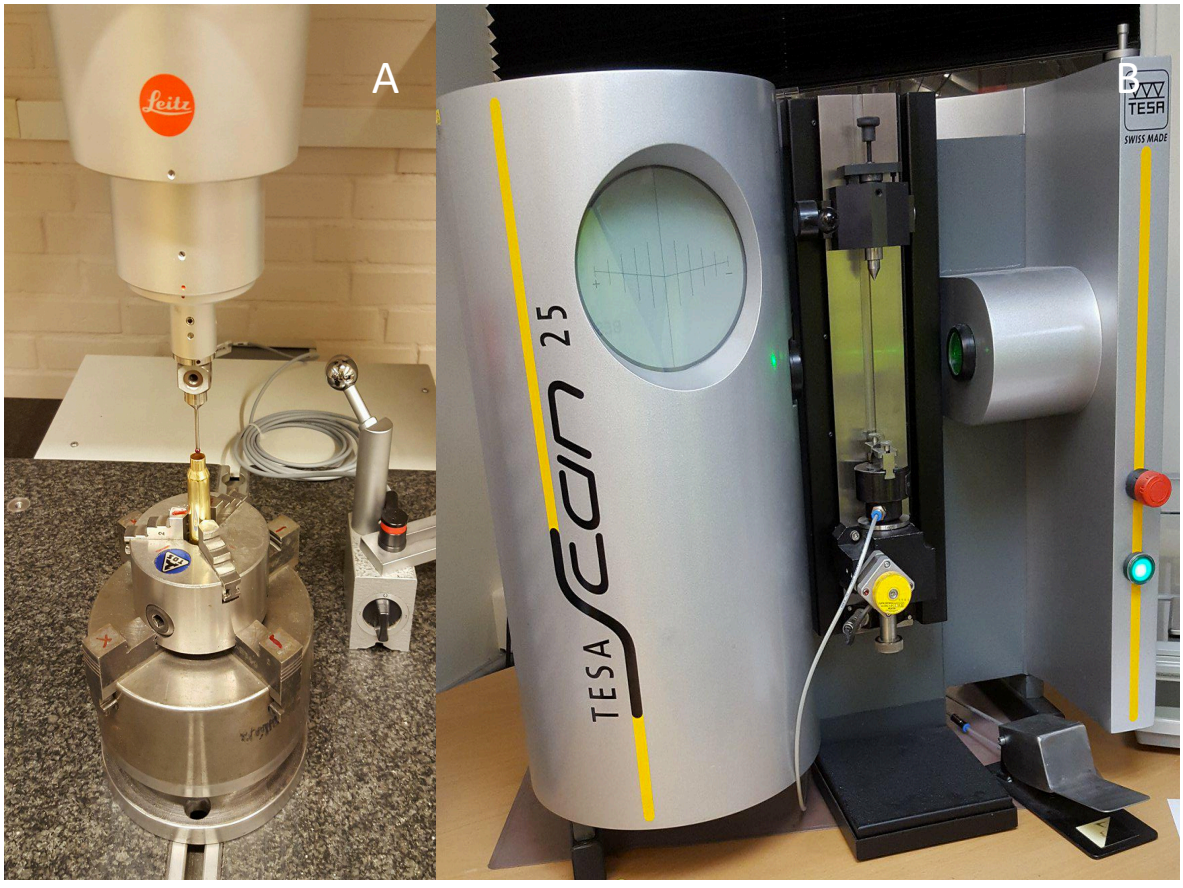

Figure 15: Measurement machines, in A is a Leitz PPM used to measure the cases and in B is a Tesa Scan 25 used to measure the bullets with cannelure.

The bullets without a cannelure was measured with a micrometer on D2 in Figure (16) of the bullet as it's done in the regular quality control. The tolerances of the bullet according to the drawing is constant of 7,83 – 0,02, in other words D1 = D2 = D3 in Figure (16), why only one measurement was made. From a total of 130 bullets 60 bullets were chosen for tensile test 1 - 3 with a diameter 7,823 ± 0,01 to keep the bullet diameter constant. For tensile test 4 and 5 the bullets were randomly selected. The bullets with cannelure was measured using a TESA Scan 25 seen in Figure (15) B, that were programmed for the specific bullet. Three measurements were made seen in figure to establish the effect of the pressed cannelure. The measured bullets were randomly selected for tensile test 6 – 11.

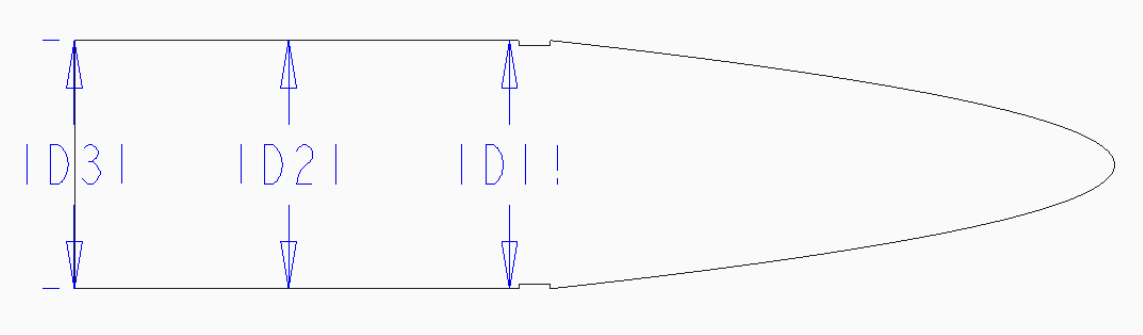

Figure 16: Measurements of bullets with cannelure in Tesa Scan 25.

4.4 Loading

The loading is made in three steps, first a primer is inserted and controlled by a special machine seen in Figure (19), then gun powder is inserted and then the bullets are pressed into the cases with the loading machine seen in figure (17).

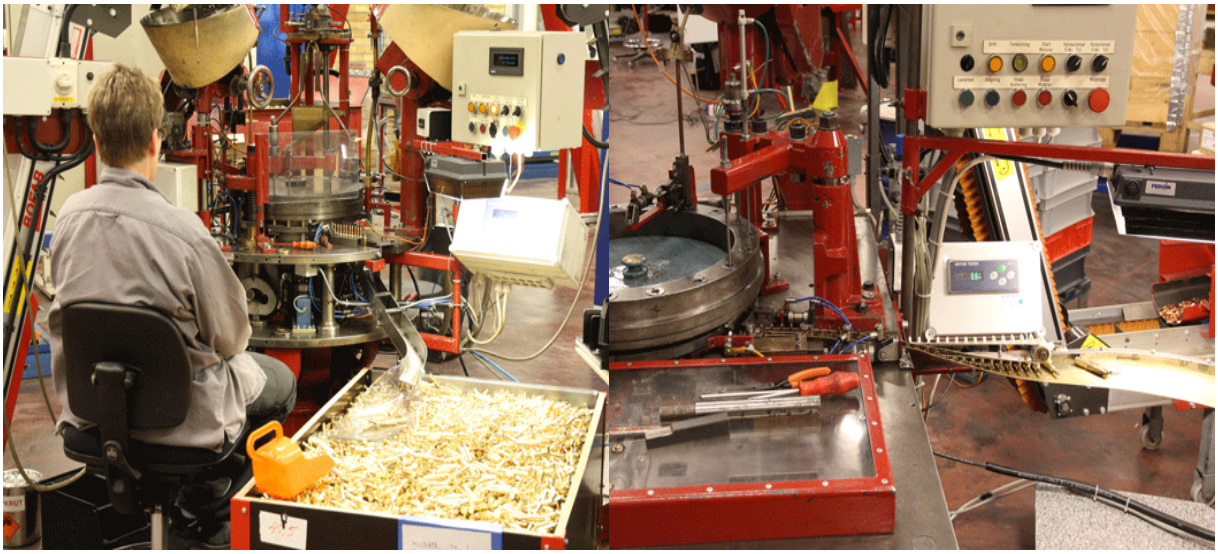

Figure 17: The loading machine used for 300-Winchester-Magnum. [25]

4.5 Tensile tests

The tensile tests were made with the machine seen in Figure (18) A, with the special jig in B.

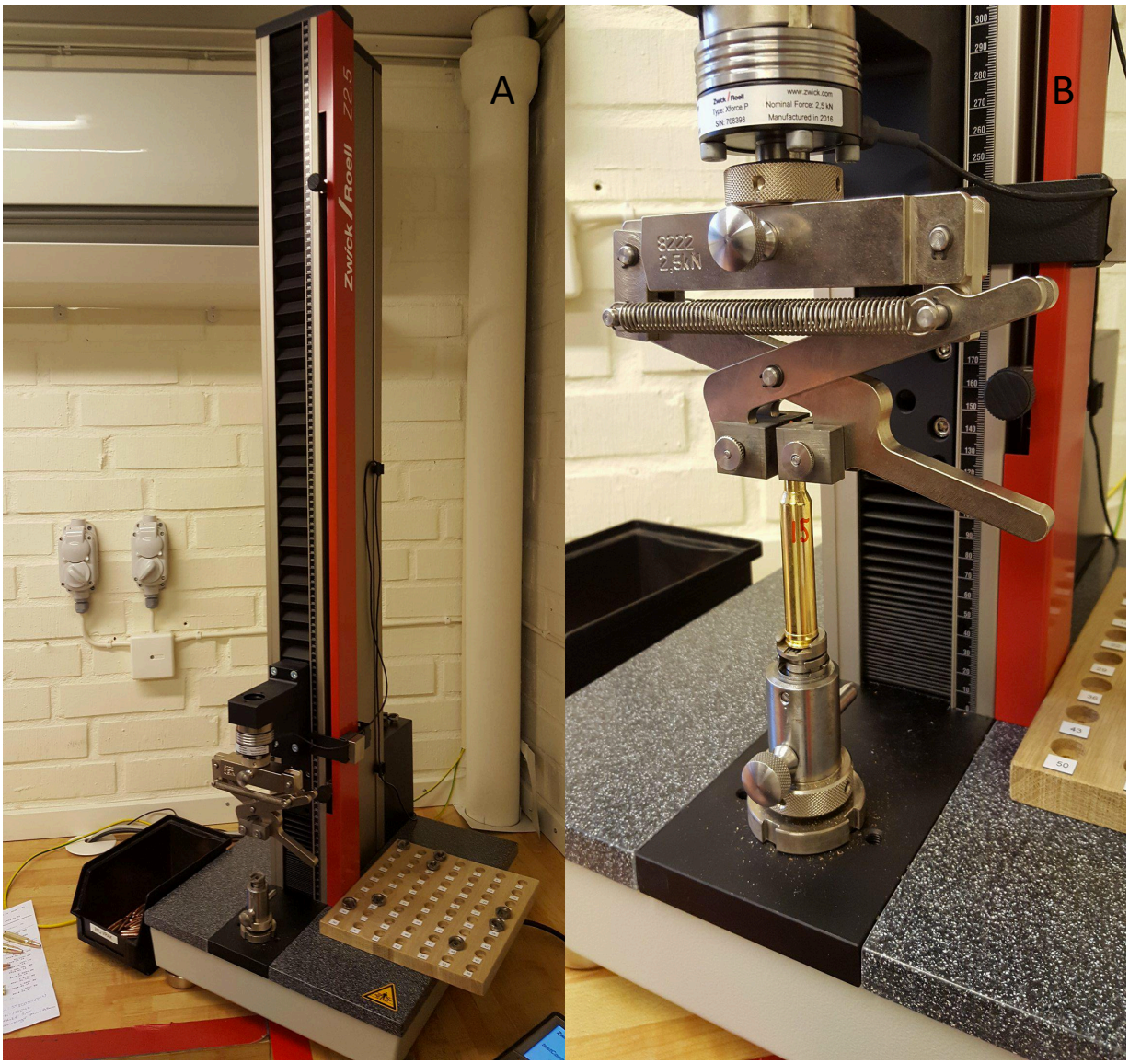

Figure 18: Zwick/Roell Z2.5 that were used for the tensile tests. In A an overview of the machine is seen and in B the special jig used.

The different parameters changed from the manufacturing process for each tensile test seen in Table (3).

Table 3: Varied parameters of tensile test 1-10.

Bullet: 30 Tip Strike	Case: 300-Winchester-Magnum										
	Cannelure		Surface treatment			Material origin		Tool change		Loading	
Tensile test	With	Without	Passivated	No Passivation	Visual annealing	Germany	Switzerland	Before	After	Gun powder	Primer
1		✓	✓				✓	✓			
2		✓	✓			✓		✓			
3		✓	✓			✓			✓		
4		✓		✓		✓			✓		
5		✓			✓						
6	✓			✓		✓			✓		
7	✓				✓						
8	✓		✓			✓			✓		
9	✓		✓			✓			✓		✓
10	✓		✓			✓			✓	✓	✓

Another tensile test 11 was made with the same parameters as in test 10 seen in Table (3) when large variations were seen after tensile test 9 and 10, in hope to find larger maximum values to evaluate the surfaces on. The dimensions weren't assumed to be of use after examination of dimensional differences of previous result.

To investigate the cause of increase in values in curves 9, 10 and 11 in Figure (25) after insertion of primer compared to curves 6, 7 and 8 without primer. Tensile tests 12 and 13 was carried out with a case 308-Magnum that goes through a different control of the primer insertion. The main difference is that the neck of the case isn't in contact during the control seen in figure (19) A and B, after insertion of the primer that verify that it's inserted correctly. In A (used for 300-Winchester-Magnum) the measurement is made by applying a force and in B (used for 308-Winchester) by a laser. The case couldn't be loaded with 30-tip strike because the tools in the loading machine need to be changed specific for each bullet, therefore the bullet Norma full metal jacket seen in Figure (4) B that was currently manufactured with 308-Winchester was used. Tensile test 12 and 13 was done with and without primer respectively, both with gun powder inserted.

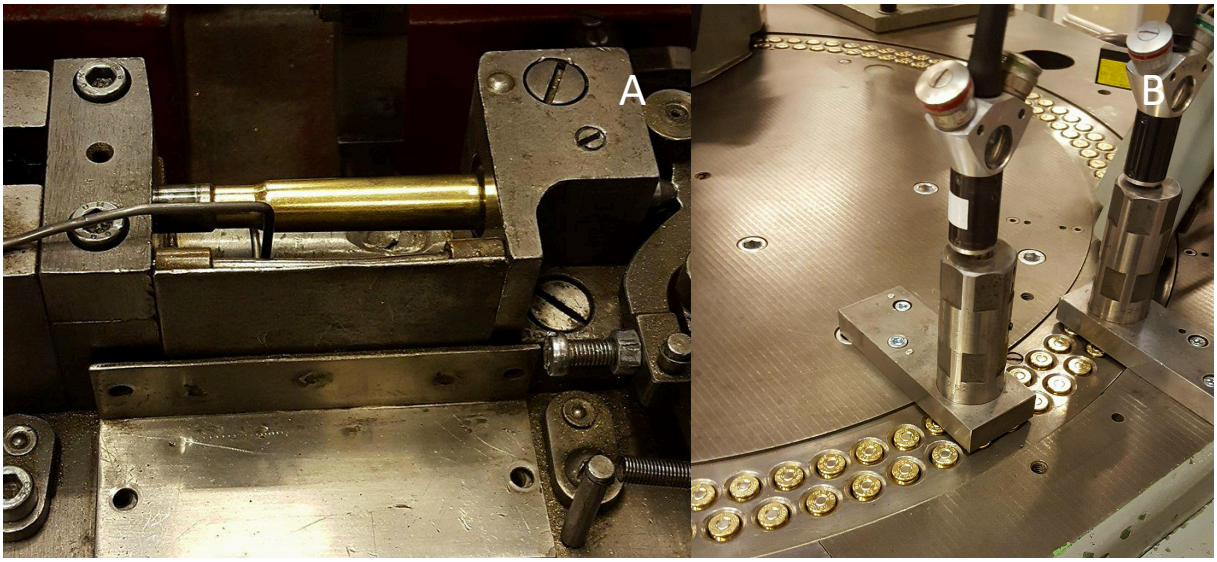

Figure 19: Measurement after primer insertion. A is used for 300-Wichester-Magnum and B is used for 308-Magnum.

4.6 Specimen preparation

4 bullets and 4 cases were chosen after the tensile test that had extreme values for the different parameters for further examination in SEM and profilometer seen in Table (4). The measured values for tensile test 1, 2 and 6 can be seen in Appendix A.

Table 4: Bullets and cases used for further examination.

Tensile test	1	2	6	11
Case	16	18	14	Maximum
Bullet	58	31	69	Maximum
Selection explanation	Bullet and case with the lowest overall tensile force.	Bullet and case with the largest tensile force of bullets without cannelure.	Bullet and case with the largest tensile force for non-passivated surface.	Bullet and case with the largest overall tensile force.

To see inside the neck of the case, all 4 cases was cut into two pieces and were cleaned with alcohol from lubrication used during the cutting.

4.7 Scanning Electron Microscopy (SEM)

The cases and bullets from Table (4) were examined in SEM to identify different surface and wear characteristics. One half of the neck of the case and the whole bullets was evaluated at different places. Pictures from the series that showed distinct characteristics was chosen to be included in the report.

4.8 Profilometer

A profilometer was used to evaluate the wear depth of the cases and bullets in Table (4). One half of the neck of the case and the whole bullets was placed in the profilometer and a 3D pictures was scanned

4.9 Hardness

The hardness of cases with the same process parameters as in tensile test 1 - 3 was measured by Vickers method with two different loads by Richard Olsson. A more detailed method and analysis can be read in his report Variations in the Hardness and microstructure in cartridge cases at annealing. In Table (10) the cases were measured at three distances on the neck as in Figure (20) with a load of 1 kilogram. The cases were measured as manufactured. For micro Vickers measurements with a load of 10 grams the neck of the cases was cut into thin slices and were mounted into a polymer, then it was grinded in several steps. The hardness was measured in a series of 30 measurements along the thin piece of the case. In Table (10) the mean values of the measurements are presented.

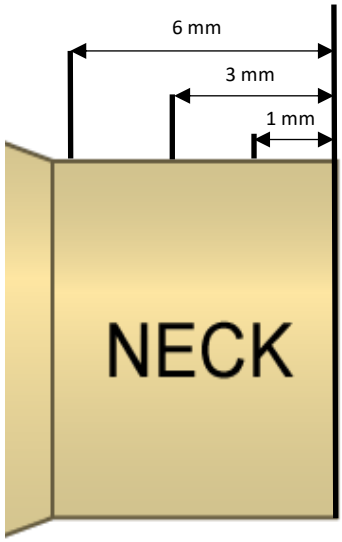

Figure 20: Hardness measurements performed with a load of 1 Kg.

The bullets from Table (10) was measured in a two series of 10 as seen in with a load of 10 grams. Some indentations couldn't be measured due to surface damages. An extra series were made on the bullet from tensile test 11 due to large extent of surface damage.

4.10 Simulations

To further investigate the results from the tensile tests and how the parameters changed varied the frictional force, simulations where made in Abaqus.

4.10.1 Dimensions

The case was modelled as an axisymmetric model as in Figure (21) A and B. The dimensions in were changed according to Table (5). The dimensions of the cases were simulated from the original drawing (excluded from the report due to company secrecy) for Case (C) 1 and 2, as a decision because only measurements of one position of the neck was made of the real cases

that it would be more precise. For C2 and C3 measurement A in Figure (21) A was decreased to simulate a plastic deformation that was suspected to be caused from the insertion of a primer. C3 was also made thicker to see how the thickness of the neck changed the frictional force, pressure and stresses.

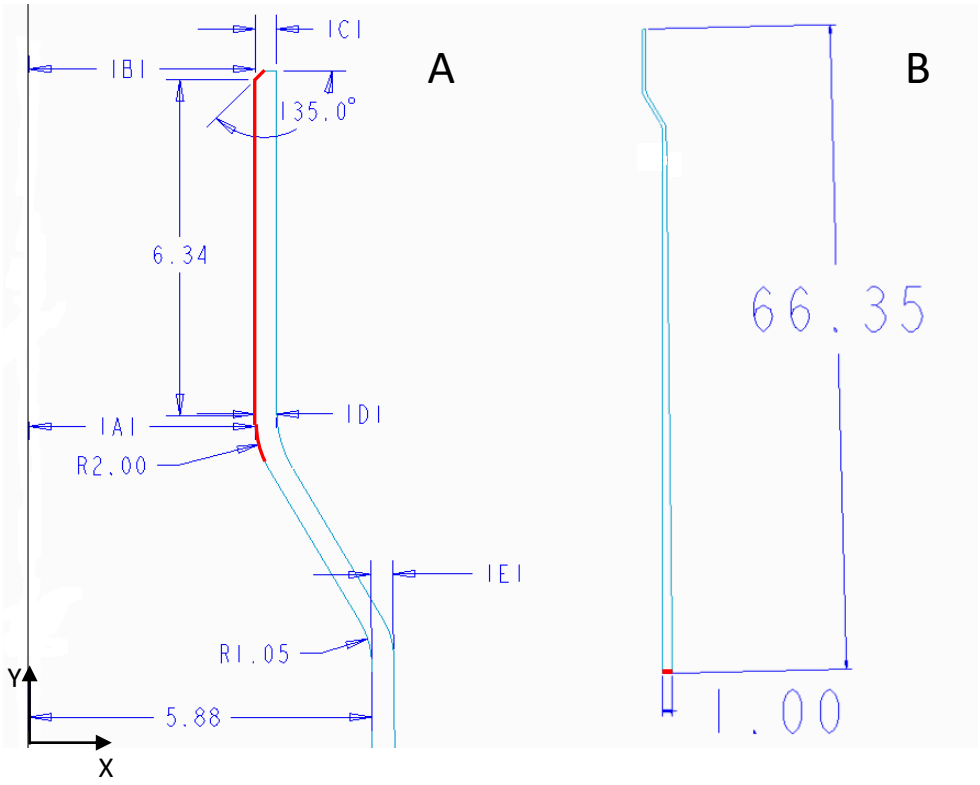

Figure 21: Dimensions of simulated cases. In A the top of the case and in B an overview.

Table 5: Dimensions for the three cases simulated from Figure (21).

Dimension	C1	C2	C3
A	3,88	3,81	3,81
B	3,88	3,88	3,89
C	0,37	0,37	0,65
D	0,37	0,37	0,67
E	0,35	0,35	0,71

The bullet simulated can be seen in Figure (22), the dimensions were changed according to Table (6). The bullet without cannerlure was according to the drawing (excluded from the rapport due to secrecy) and the bullet without cannelure was modelled according to the measured values in Table (8).

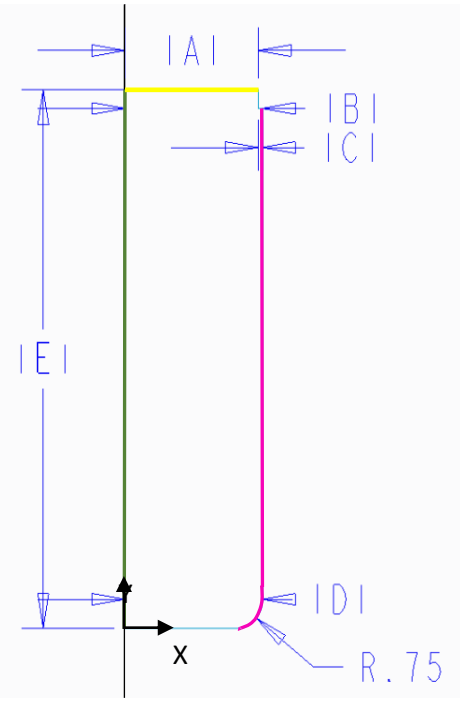

Figure 22: Dimensions of the simulated bullets.

Table 6: Dimensions of the simulated bullets.

Dimension	B1 (Without cannelure) [mm]	B2 (With cannelure) [mm]
A	3,915	3,8
B	3,915	3,92
C	0	0,12
D	3,915	3,91
E	15	15

The measurement B to D along the pink line was equal to 14 mm during the tests.

4.10.2 Material

The material was set according to Table (1) with both an elastic part and a plastic part with a table calculated in Matlab by Equation (7).

4.10.3 Contact

The X-axis of the bullet was translated to top of the case. The red line on the case in Figure (21) was set as the slave surface and the pink line in Figure (22) was set as the master surface. Interaction was set between the surfaces with normal behavior as hard contact and tangential behavior as penalty with a frictional coefficient of 0,14. The frictional coefficient was assumed according to the section 3.1 and by comparing with the results in Figure (25) and assuming that the simplified model should yield lower values due to no adhesion or plastic deformation of the surfaces.

4.10.4 Boundary conditions and mesh

The case was set to encastre along the red line in Figure (21) B and no allowed displacements was set along the Y-axis on the bullet in Figure (22) in the X-direction in the initial step. A displacement of 14,2 mm was set in step 1 along the yellow line in Figure (22), from measurements on a loaded cartridge. The displacement set in step 1 was inactivated in step 2 and a new displacement set to 0 mm was created on along the yellow line. The models were simulated with 2300 – 2500 elements after a convergence study of SM1, with a mesh of 0,1 mm along the slave and master surfaces that grew bigger up to the global seeds of 1 mm. The models were meshed with hexagonal elements.

4.10.5 Simulations

Four different simulation models were made with the case and bullet combinations seen in Table (7).

Table 7: Simulating models corresponding to dimensions in Table (5) and Table (6).

Simulation Model	SM1	SM2	SM3	SM4
Case	B1	B1	B2	B2
Bullet	C1	C2	C1	C3

In SM3 the hardening parameter η was changed until too large plastic deformation for the model to converge, to investigate how the hardening of the material affected the frictional force.

The plots were created by summing the reaction forces in the Y-direction along the yellow line in Figure (22).

To further evaluate the cartridges with the largest maximum frictional force in SM3 and SM4, a more thorough investigation was made. The stresses, displacements and pressure were calculated by measurement at the top node on the 6,34 mm long part of the case in Figure (21) A. The remaining displacement after the tensile test was calculated to verify that the hardening parameters and hardening model in Equation (7) was correct.

4.11 Pressure inside the cartridge case

A possibility of an under pressure during the tensile test 9, 10, 11 and 12 with a primer inserted was suspected. The maximum pressure inside the cartridge case was therefore approximated with Equation (9) for different volumes inside the case. nRT was assumed to be constant during the loading process.

$$P_2 = \frac{P_1 V_1}{V_2} \tag{9}$$

Where P_2 and V_2 is the pressure and volume respectively in the case after loading and P_1 is the atmospheric pressure of 101,325 kPa and V_1 is the volume of the case before loading. The volume V_1 inside the case prior to loading was calculated in Creo Parametric from measurements from the real drawing to 7 884 mm^3. The force exerted on the bullet was calculated with bottom area A_{Bullet} = 48,28 mm^2 inside the case as seen in Equation (10) and by subtracting the atmospheric pressure to P_2, by assuming that the pressure is zero for loaded pressure and that the suspected negative pressure created during the tensile test is equal to the pressure calculated by compression.

$$F_{Bullet} = (P_2 - P_1)A_{Bullet} \tag{10}$$

F_{Bullet} was plotted against V_2 to see how a decreased volume increases the force exerted on the bullet.

4.12 Press fit

The pressure between the bullet and the case was calculated as a simplified elastic model as in Figure (23) to further understand which parameters affects the frictional force and to further verify the simulation model.

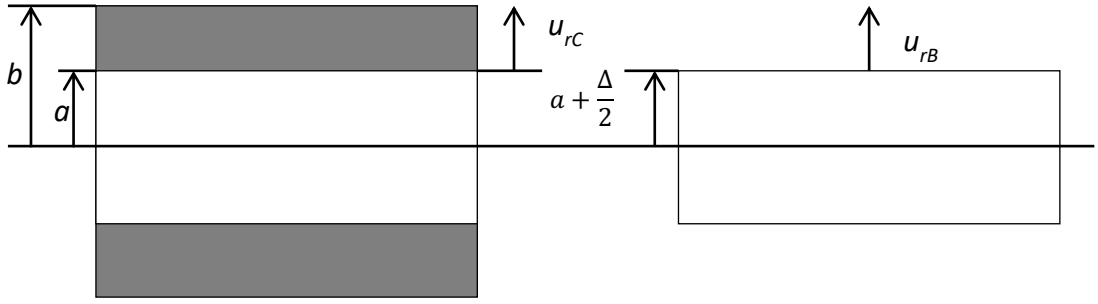

Figure 23: Elastic model to calculate the pressure between the bullet and the case.

The radial stresses set according to [26], they were then set to zero and -p as in Equation (11) and Equation (12).

$$\sigma_r(r = b) = A - \frac{B}{b^2} = 0 \tag{11}$$

$$\sigma_r(r = a) = A - \frac{B}{a^2} = -p \tag{12}$$

Equation (11) and Equation (12) was then reorganized as in Equation (13).

$$A = -\frac{a^2}{a^2-b^2}P \text{ and } B = -\frac{a^2b^2}{a^2-b^2}P \tag{13}$$

The displacement U_{rC} in the radial direction from Figure (23) is:

$$u_{rC}(r=a) = \frac{1}{E}(A(1-\nu)a + B(1+\nu)\frac{1}{a}) \tag{14}$$

Equation (13) ➔ Equation (14)

$$u_{rC}(r=a) = \frac{(1-\nu)}{E}\frac{a^3}{b^2-a^2}p + \frac{(1+\nu)}{E}\frac{ab^2}{b^2-a^2}p \tag{15}$$

The displacement for the bullet was approximated to zero as its solid and will be very small compared to the displacement of the case. This gives the displacement of the case:

$$u_{rC}(r=a) = \frac{\Delta}{2} \tag{16}$$

Equation (15) ➔ Equation (16)

$$p = \frac{\Delta}{2}\frac{E(a^2-b^2)}{a^3(\upsilon-1)-(ab)^2(1+\upsilon)} \tag{17}$$

The pressure between the case and the bullet was calculated by Equation (17). In the calculation a = 3.9 mm from the measured values and b = 4,23 mm. The displacement Δ = 0,02 from the largest measured values of the bullet.

5 Results

5.1 Measurements

In Table (8) the mean values of the dimensional measurements are presented.

Table 8: Measurements of bullets and cases for tensile test 1-10.

Tensile test		1	2	3	4	5	6	7	8	9	10
Case	$d1_{Case}$ [mm]	7,80	7,80	7,80	7,79	7,79	7,80	7,80	7,80	7,80	7,80
	$D1_{Case}$ [mm]	8,46	8,45	8,45	8,45	8,46	8,46	8,46	8,46	8,46	8,45
	$d2_{Case}$ [mm]	7,83	7,83	7,83	7,86	7,85	7,85	7,85	7,83	7,83	7,83
	$D2_{Case}$ [mm]	8,49	8,49	8,49	8,51	8,52	8,52	8,52	8,49	8,5	8,49
	C1 [mm]	0,019	0,018	0,016	0,017	0,016	0,019	0,028	0,023	0,018	0,021
	C2 [mm]	0,020	0,021	0,020	0,019	0,017	0,018	0,014	0,017	0,016	0,020
	Weight (g)	14,04	14,05	13,96	13,98	13,97	14,00	13,96	13,99	13,99	13,99
Bullet without cannelure	D2 [mm]	7,83	7,82	7,82	7,82	7,82	-	-	-	-	-
	Weight (g)	11,03	11,03	11,03	11,03	11,03	-	-	-	-	-
Bullet with cannelure	D1 [mm]	-	-	-	-	-	7,83	7,83	7,83	7,83	7,83
	D2 [mm]	-	-	-	-	-	-	-	-	7,83	7,83
	D3 [mm]	-	-	-	-	-	7,81	7,81	7,81	7,81	7,81
	Weight (g)	-	-	-	-	-	11,01	11,01	11,06	11,00	11,01

In Figure (24) the differences between the average of the measured values before and after the tensile tests for each series is showed. $\Delta dCase = d2_{Case}-d1_{Case}$, $\Delta C=C2-C1$ and $dh= d2_{Case}-D2$ (for bullet without cannelure) and $dh= d2_{Case}-D3$ (for bullet with cannelure).

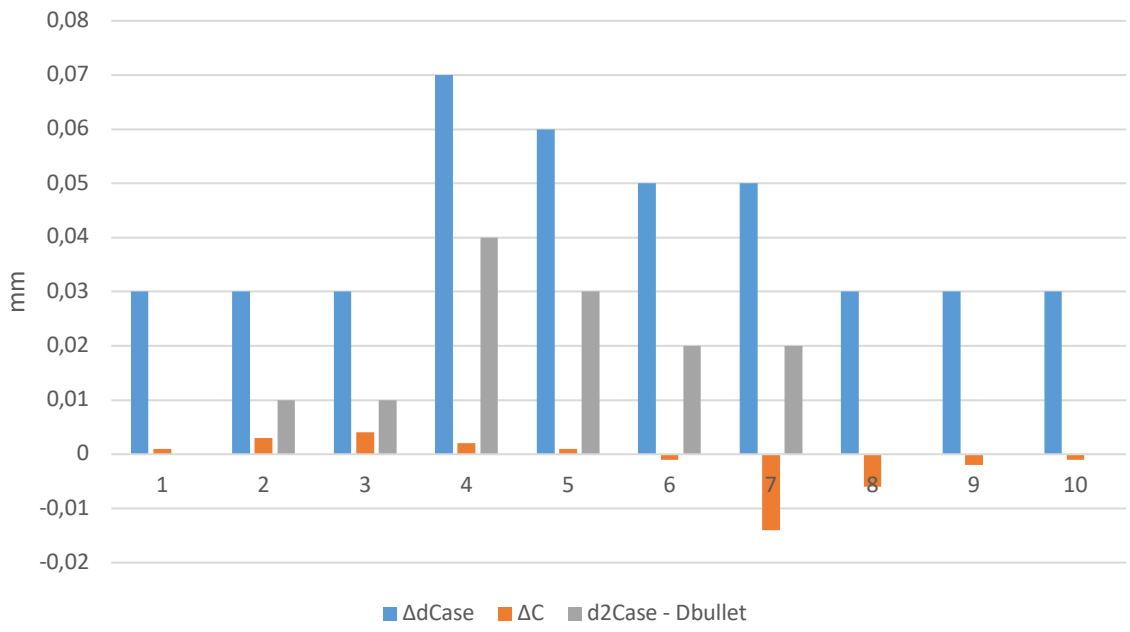

Figure 24: Comparison of measurements from Table (8).

5.2 Tensile tests

In Figure (25) the frictional force measured in Kilogram by the tensile test machine described in Section 4.5 can be seen.

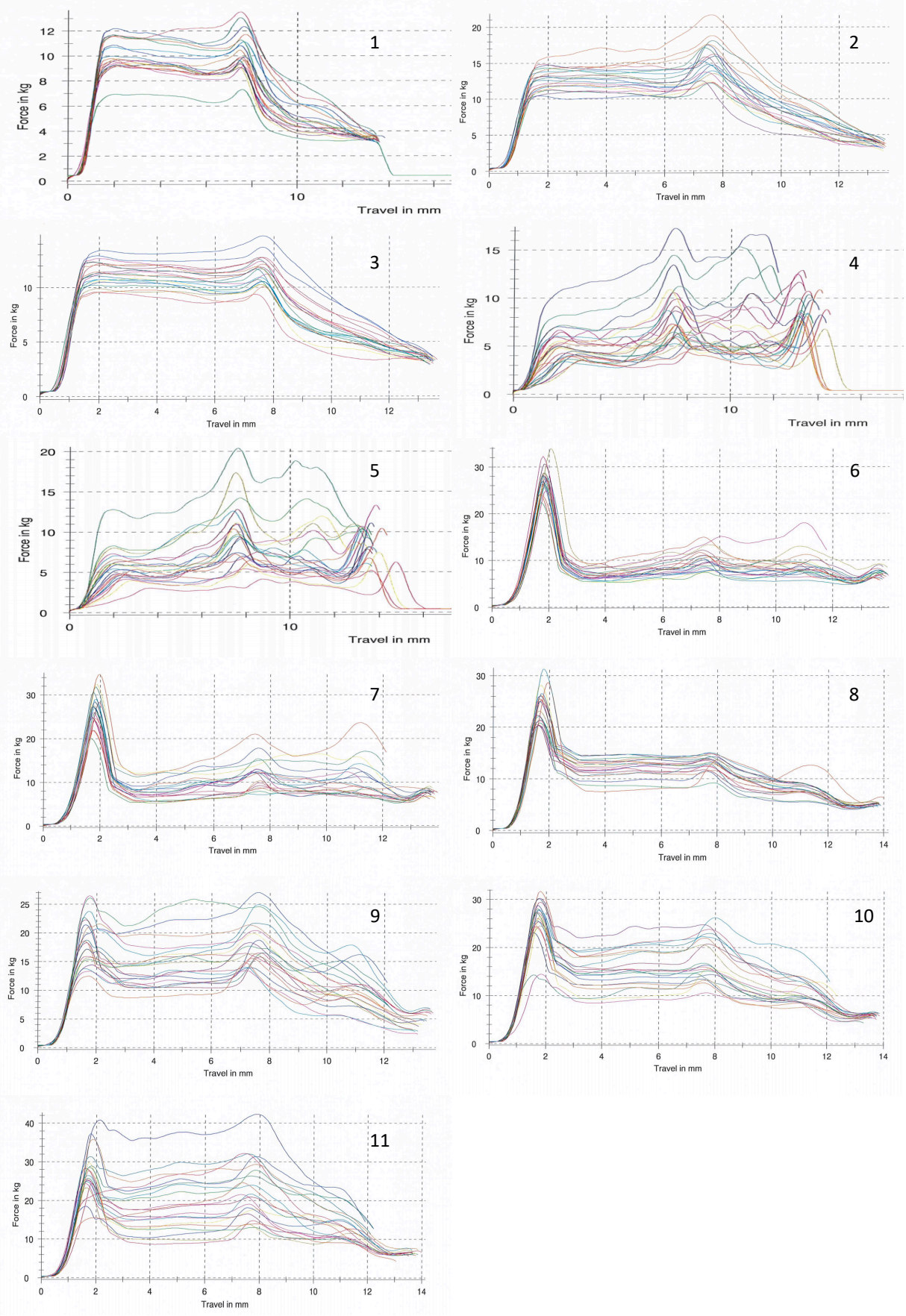

Figure 25: Tensile test 1-10 with 300-Winchester-Magnum with the bullet 30 Tip Strike measured in Kilogram.

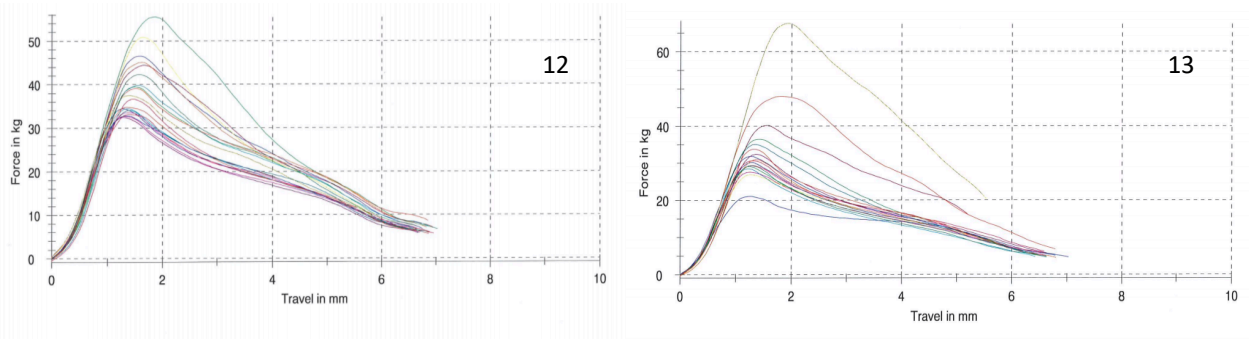

Figure 26: Tensile test 12 and 13 with the case 308-Winchester with the bullet Norma full metal jacket, measured in Kilogram.

In Table (9) the average value and extreme values of the frictional force from tensile test 1-13 can be seen.

Table 9: Average, maximum and minimum forces from tensile tests 1-13.

Tensile test	1	2	3	4	5	6	7	8	9	10	11	12	13
Favg	10,5	15,3	11,7	10,2	11,0	27,5	27,0	24,1	19,9	25,9	28,3	39,0	33,9
Fmax	13,5	21,7	14,7	17,3	20,4	33,9	34,8	31,2	27	31,8	42,3	55,5	67,8
Fmin	7,3	12,2	9,6	6,8	6,3	22,4	20,1	20,3	13,4	14,5	18,5	32,6	21

5.3 SEM

In Figure (27) the result from the SEM examination can be seen with the cases from Table (4). A is case from tensile test 11, B is the case from tensile test 6, C is the case from tensile test 2 and D is the case from tensile test 1. In A and B areas where adhesion and transfer of material from the bullets to the case during the tensile test or the loading are circled in red.

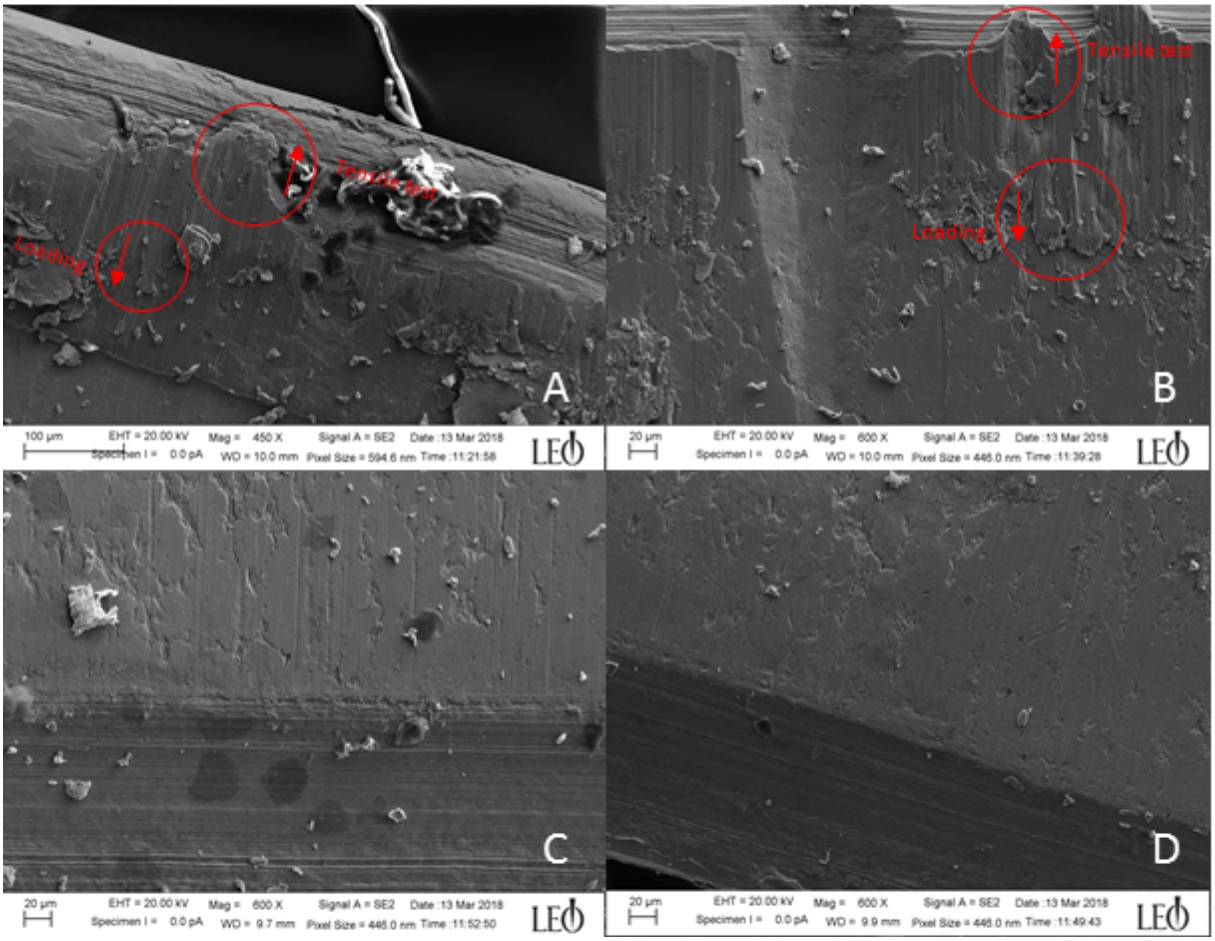

Figure 27: Pictures of the cases in Table (4) from SEM.

The bullets examined in SEM can be seen in Figure (28). A, B and C are the pictures of the bullet from tensile test 11. D, E and F are the pictures of the bullet from tensile test 6. G, H and I are the pictures of the bullet from tensile test 2. J, K and L are the pictures of the bullet from tensile test 1. The pictures to the left (for example A) are the pictures of the bottom part of the bullets, the pictures in the middle are the middle part and the pictures to the left (for example C) are the upper part of the bullet that been in contact during the tensile tests.

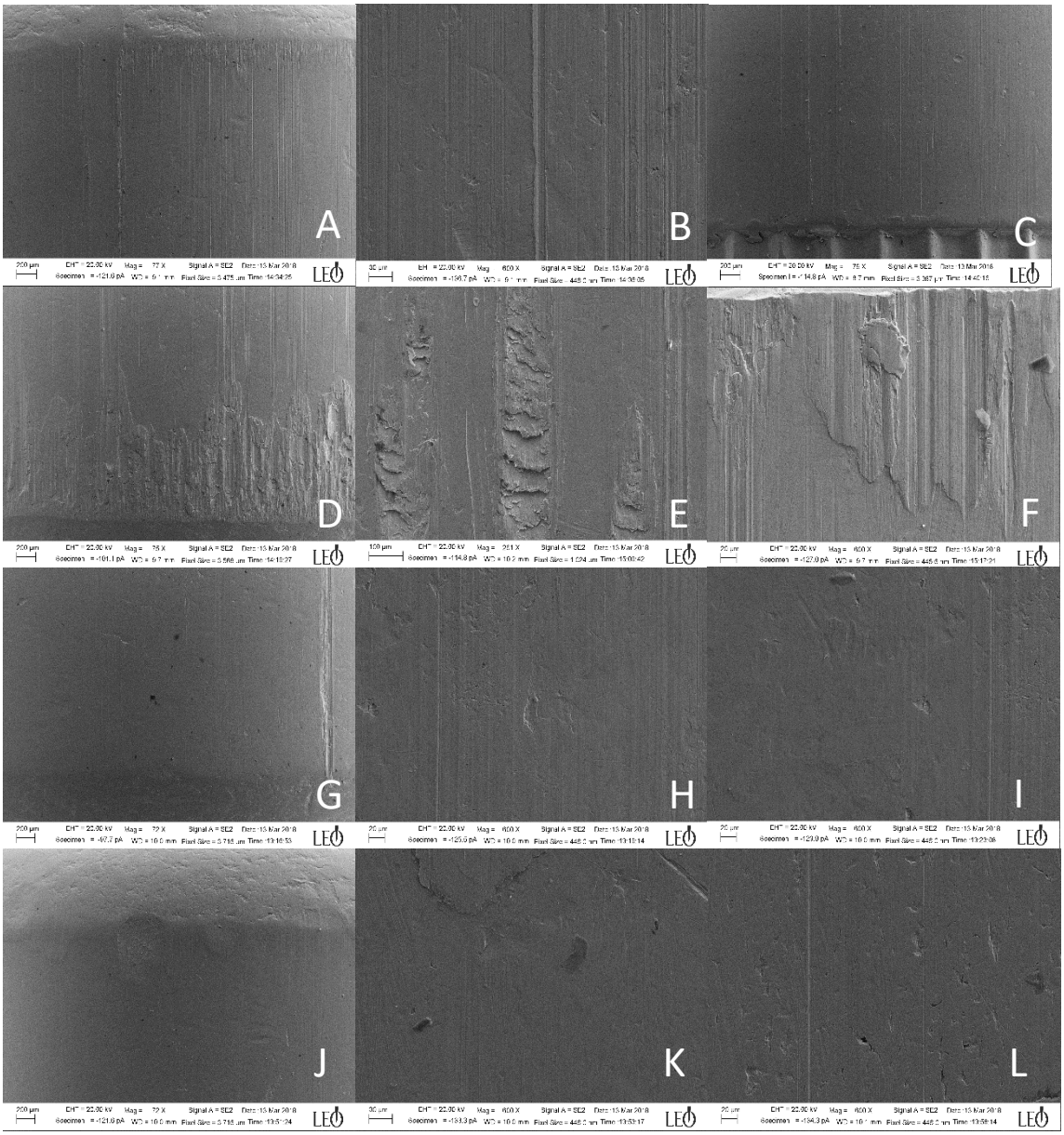

Figure 28: Pictures from SEM of the examined bullets in Table (4).

5.4 Profilometer

In Figure (29) the results of the cases from the profilometer can be seen. A and B are the pictures of the case from tensile test 11. C and D are the pictures of the case in tensile test 6. E and F are the pictures from tensile test 2. G and H are the pictures from tensile test 1.

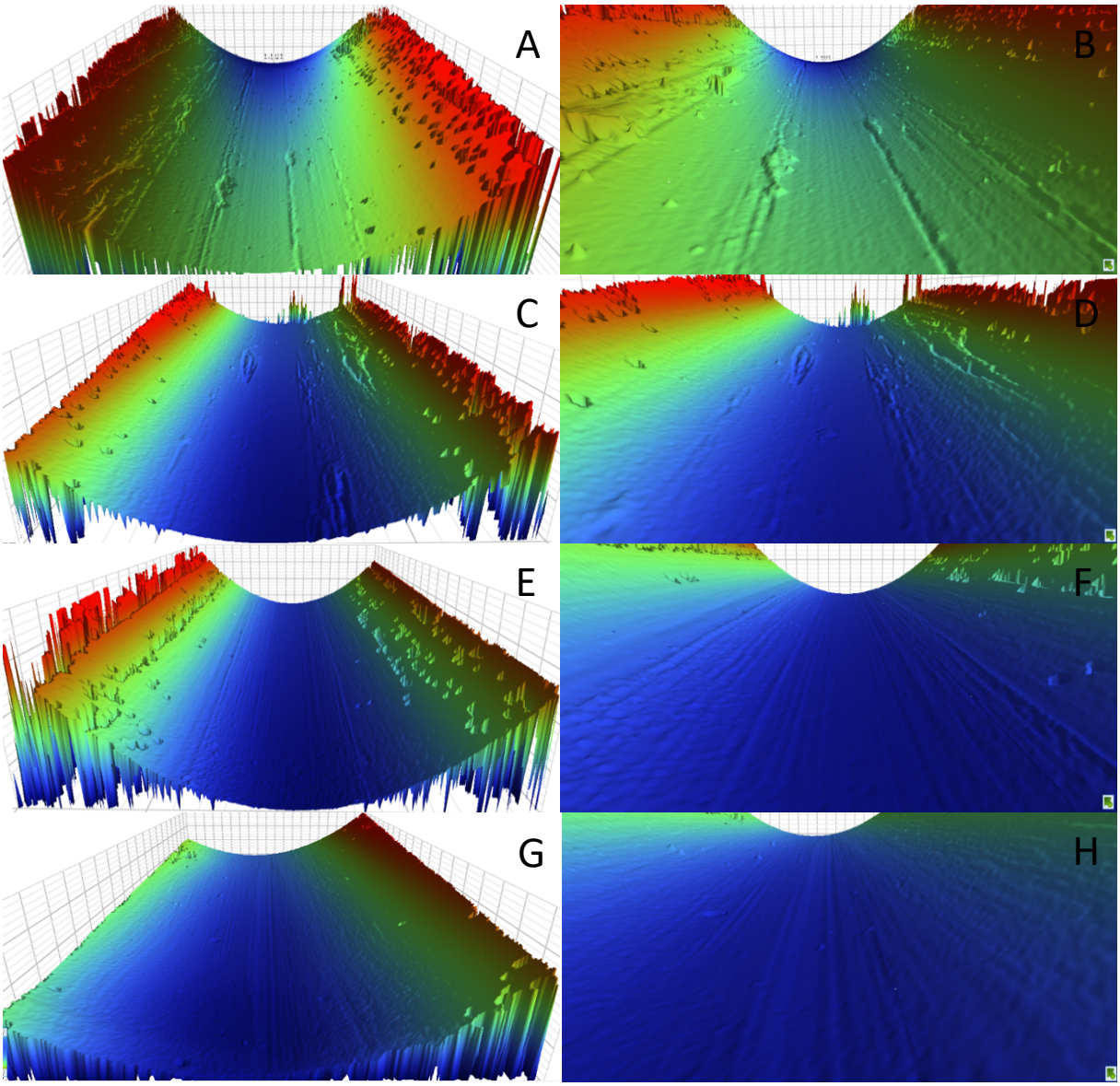

Figure 29: 3D pictures of the cases in Table (4) from the profilometer.

In Figure (30) the results of the bullets from the profilometer can be seen. A and B are the pictures of the bullet from tensile test 11. C and D are the pictures of the bullet in tensile test 6. E and F are the pictures of the bullet from tensile test 2. G and H are the pictures of the bullet from tensile test 1.

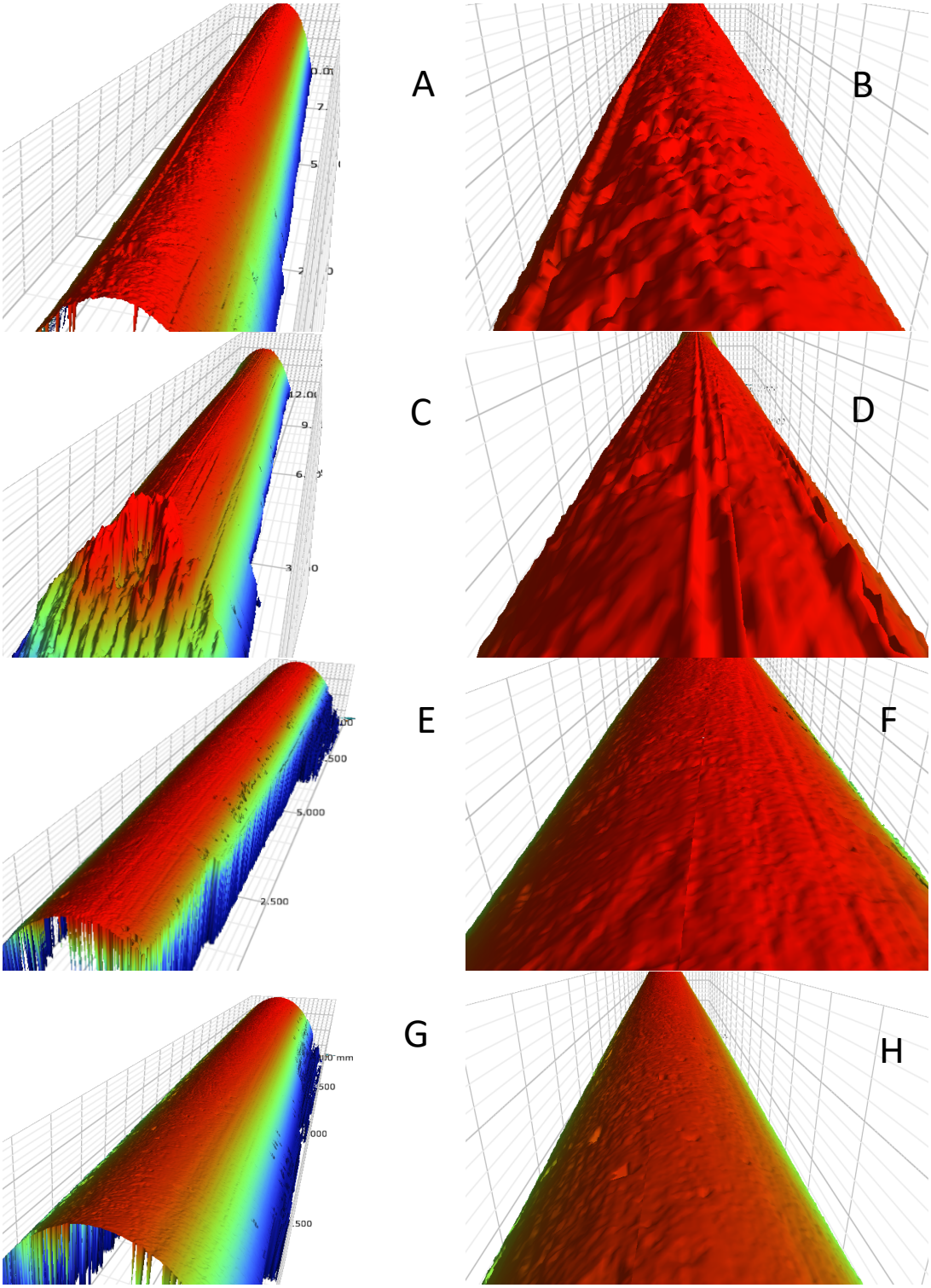

Figure 30: 3D pictures of the bullets in Table (4) from the profilometer.

5.5 Hardness

In Table (10) average hardness values by Vickers method can be seen for the two different loads used.

Table 10: Hardness of 300-Winchester-Magnum after the final annealing, prior to passivation.

Material origin	**Switzerland**			**Germany**			**Germany**		
Tool change	Before			Before			After		
Distance on the case	1 mm	3 mm	6mm	1 mm	3 mm	6mm	1 mm	3 mm	6mm
Load of 1 Kilogram	104,5	108,5	115,4	107,7	111,8	118,2	103,4	106,5	114,8
Load of 10 grams	167,3			184,5			176,5		

The hardness measured hardness of the bullets varied in average between 155-156 Hv. The complete hardness measurements can be seen in Appendix B.

5.6 Simulations

In Figure (31) the simulation with SM1 can be seen. The force drops suddenly to zero when the bottom of the bullet passes the bottom of the neck in the case.

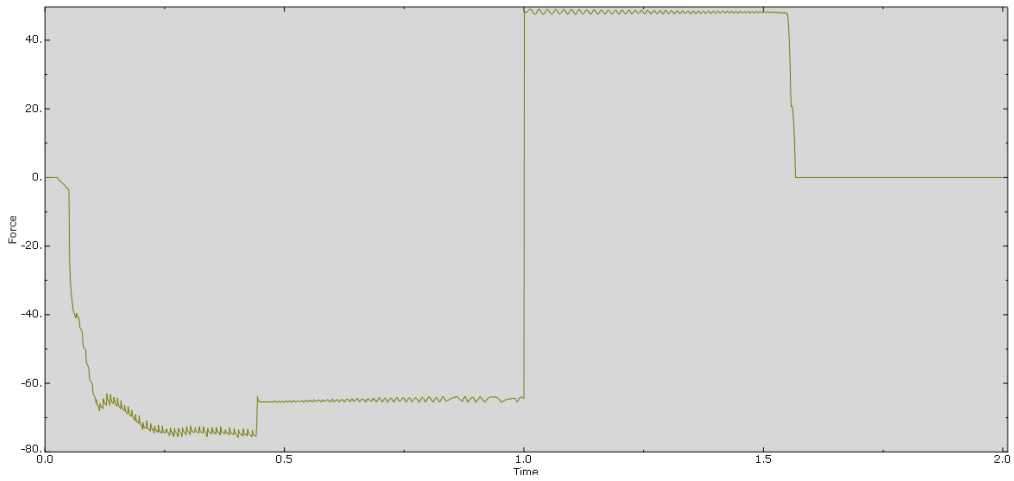

Figure 31: Plot of reaction forces for simulation model 1.

In Figure (32) the simulation with SM2 can be seen. The force has an increase when the bottom of the bullet goes through the bottom of the neck in the case.

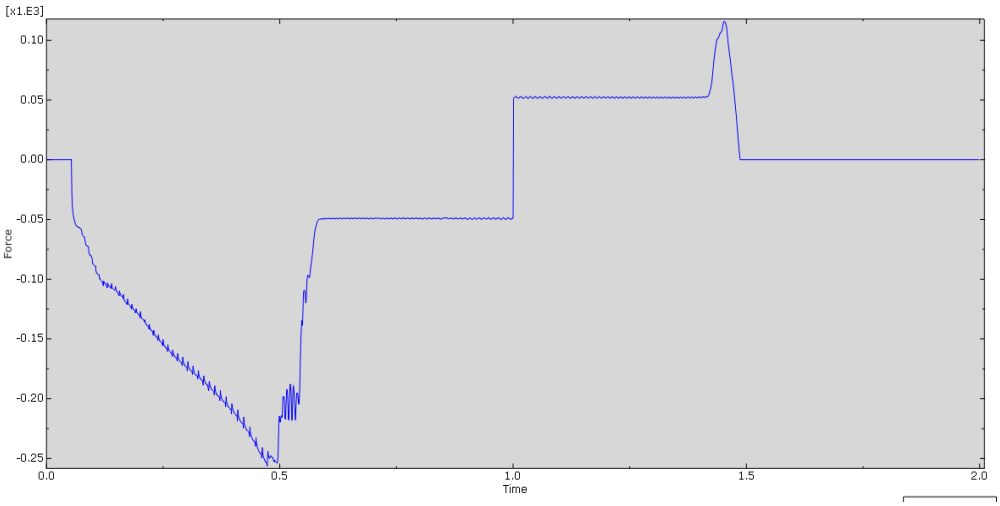

Figure 32: Plot of reaction forces from simulation model 2.

In Figure (33) the simulation with SM3 can be seen. An increase in the maximum frictional force due to the increase in diameter of the top of the bullet and a small increase in force after time 1,5 due to deformation in the bottom of the bullet as seen in Figure (34) was noted.

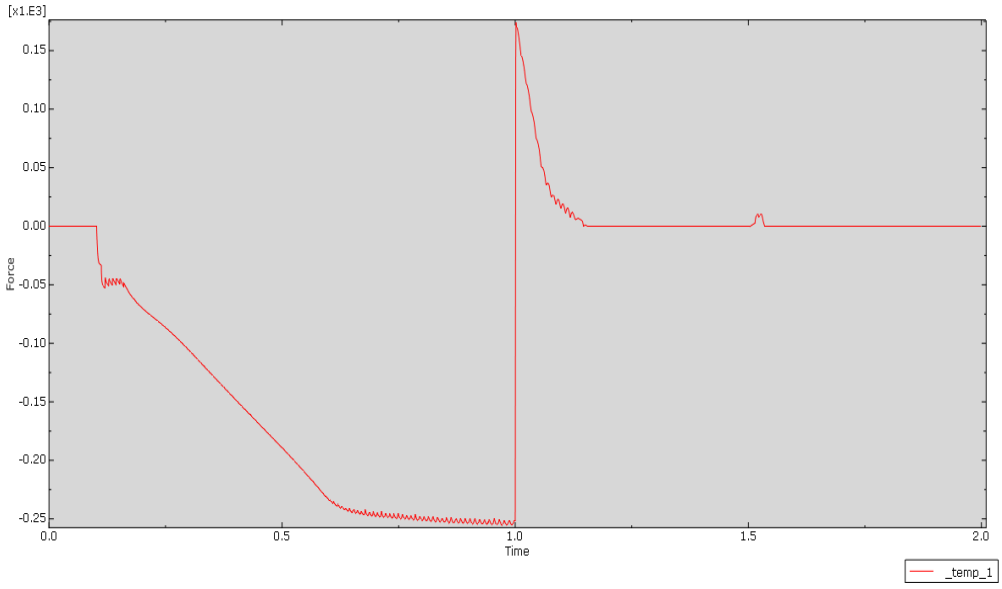

Figure 33: Plot of reaction forces from simulation model 3.

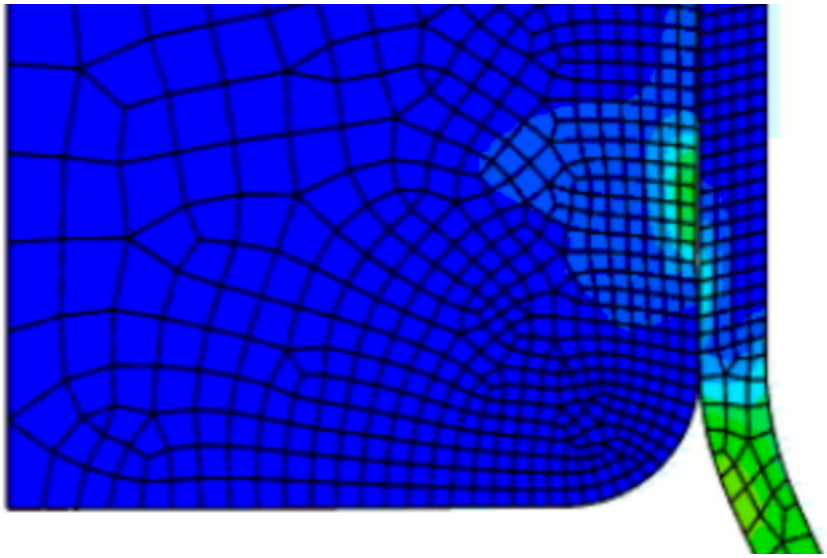

Figure 34: Shows the deformation of the bullet that causes the force increase at time over 1.5 seconds in Figure (33).

The hardening parameter η was varied according to Table (11). The maximum summed reaction force is shown for each test.

Table 11: The results from SM3 with different hardening coefficient on the bullet and the case.

η_{Bullet}	η_{Case}	FMAX [N]
0,54	0,49	170
0,54	0,4	197
0,54	0,3	283
0,4	0,49	191
0,3	0,49	211
0,6	0,49	168

In Figure (35) the Von Mises stress in A and pressure in B between the bullet and the case from SM3 is showed in MPa. A further comparison between SM3 and SM4 is showed in Table (12).

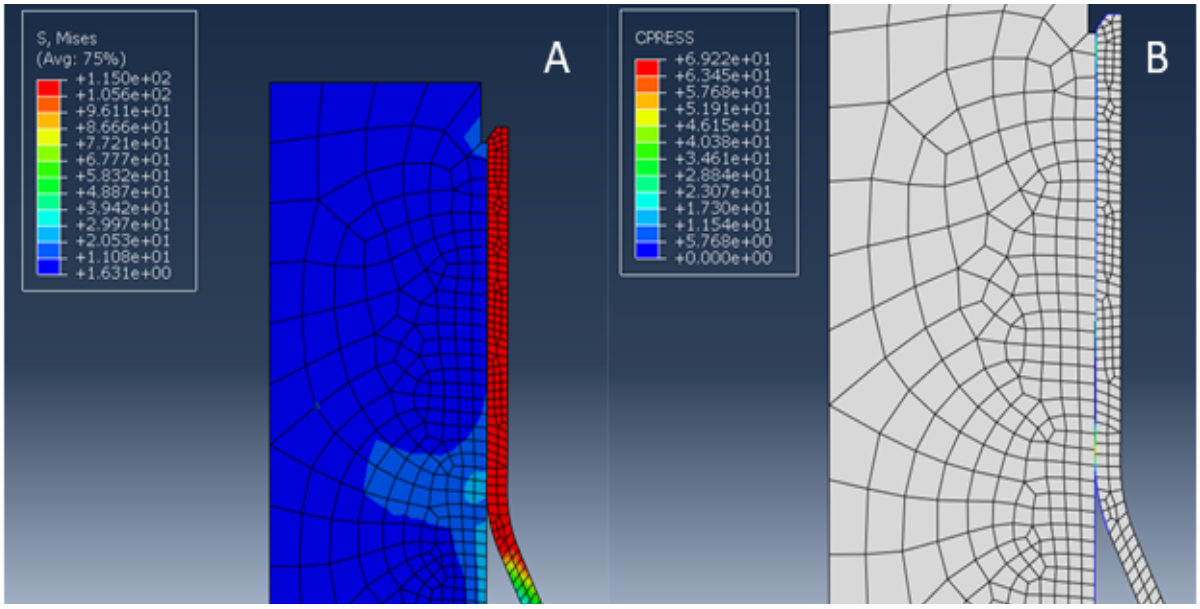

Figure 35: Von mises stress in A and pressure in B from SM3.

In Figure (36) the simulation with a thicker neck if the case according to measurements in SM4 can be seen. An increase in the maximum frictional force, but without the small increase due to plastic deformation of the bullet was noted.

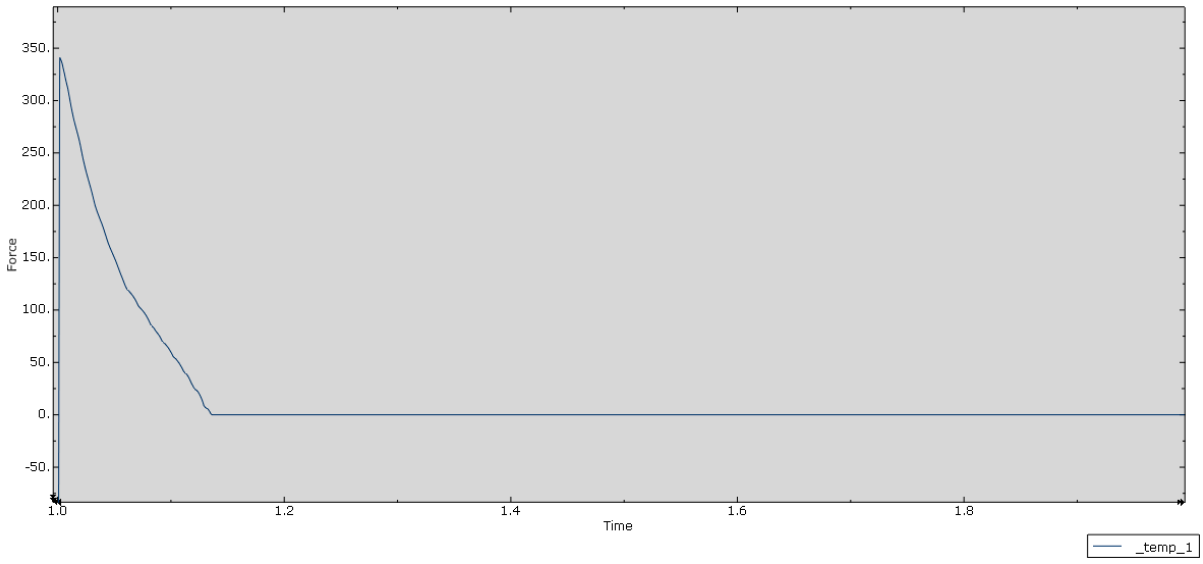

Figure 36: Plot of the reaction forces from simulation model 4

In Figure (37) the stresses and pressure between the case and bullet from SM4 in MPa. Note that the stress concentration at the bottom in A corresponds to the highest pressures in B.

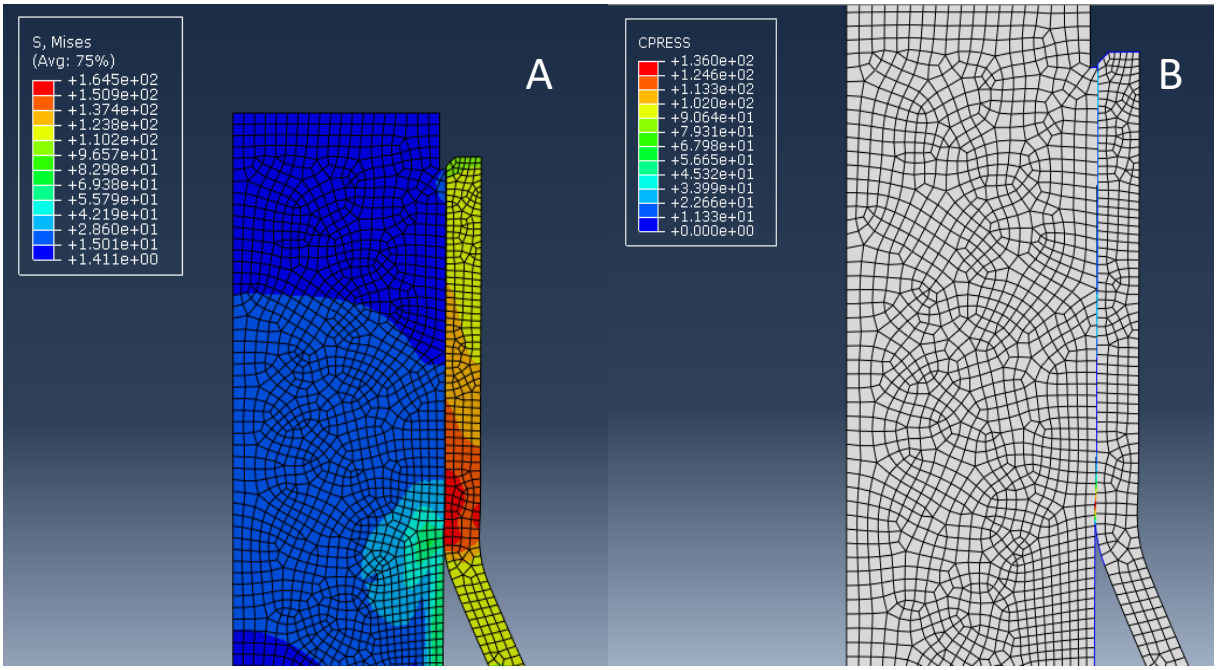

Figure 37: The von mises stress and pressure between the bullet and case from SM4.

To validate the hardening parameters and to discover differences between a thicker and a thinner case, the deformation at the top of the case was measured for SM3 and SM4. The maximum displacement and the remaining displacement (which is the plastic deformation of the case) was noted seen in Table (12).

Table 12: Comparison of stress, displacement and pressure between SM3 and SM4.

Simulation model	Maximum stress (V.M) [MPa]	Maximum displacement [mm]	Remaining displacement [mm]	Maximum pressure [MPa]	Minimum pressure [MPa]
3	115	0,052	0,045	69	5,7
4	165	0,043	0,035	136	11

5.7 Pressure inside the case

In Figure (38) the variations in force due to pressure plotted with Equation (10). It can be seen that the force increases rapidly below volumes of 200 mm^3.

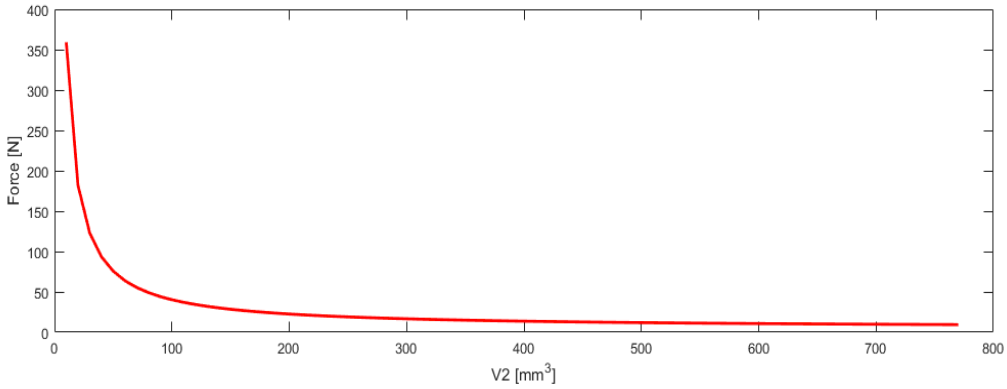

Figure 38: The variations in force on the bullet inside the case of different volumes after loading.

5.8 Press fit

The pressure between the case and the bullet according to the simplified elastic model was calculated to by Equation (17) to p = 9.45 MPa.

6 Discussion

6.1 Measurements

As seen in Figure (24) some trends were found connected to the different parameters changed. The difference in inner diameter of the case and the difference between the inner diameter after the tensile test and the diameter of the bullet is larger for all non-passivated surfaces. The reason for this is assumed to be caused by the loading procedure after examination of the bullets and cases visually, in SEM and profilometer. The bullet with the non-passivated surface had large deformations and wear at the bottom of some bullets seen in Figure (30) C. When the bullet is placed on the top case before being pressed into it, it's randomly if the central axis of the bullet line up with central axis of the case. This random element of the loading in combination with a rougher surface on the non-passivated cases is assumed to cause this extra plastic deformation. The process were the bullet is placed on top of the case is not visual, this couldn't be verified.

It's also seen in Figure (24) that the concentricity is less after the tensile test for all bullets with a cannelure. This is due the fact that the largest diameter of the bullet is at the top which produces an even deformation around the neck of the case which decreases the concentricity. This was suspected to cause a tight seal that could create the buildup of an under pressure after insertion of the primer. This theory is explained later in the discussion.

6.2 Tensile tests

The change of material origin and tools between curve 1-3 mainly resulted in a higher average value for the cases with German material and new tools. As seen in Table (10) the hardness is higher both with 1 kg and 1 g and have some values significantly higher. The effect of the hardness that suppresses the plastic deformation have been showed in the simulations (as is explained more in detail later in the discussion) to have an effect on the frictional force.

It's a clear difference between curve 1-3 and 4-5 which have passivated and non-passivated surfaces respectively, where the curves for the non-passivated is not as continuous. This is suspected to be caused by the change from dry to lubricated wear and the change from mainly abrasive ploughing to mainly cutting. This can be seen from the non-passivated case with a bullet with cannelure in SEM and the profilometer which had severe wear.

In tensile test 6-8 the effect of the passivation film was evaluated further. The passivated surface in tensile test 8 showed similar results to the cases with non-passivated surface in test 6 and with visual annealing in test 7, which had been passivated but annealed afterwards. The meaning of these tests was to see if larger frictional forces would be seen due to adhesion in tensile test 7. A theory was that the passivation film on the cases with visual annealing would prevent some shelter against oxidation during the annealing. The tensile tests showed that no variations between the non-passivated and the ones with visual annealing which means that the passivation film is completely or almost completely burnt off and don't prevent oxidation. It can also be seen that the cannelure gives continuous curves which is comparable to the passivated surfaces, which was not the case for the bullets and cases without a cannelure. The force doesn't increase by the absence of boundary lubrication because the asperities penetrates the passivation film seen in SEM and the profilometer, due to the small increase in bullet diameter. It can be seen from the measurements that all tensile test with non-passivated

cases had larger plastic deformation of the neck. The increased plastic deformation is also assumed to minimize the effects of dry sliding compared to lubricated why no difference in force can be seen.

The behavior of tensile test 6-8 compared to 9-11 when the only difference is that the later have had a primer inserted, was suspected to be caused by a under pressure created inside the case during the tensile tests. The air inside the case that would create an over pressure during the loading was assumed to escape due to dimensional differences between the case and the bullet. A seal was assumed to be created caused by a larger diameter at the top of the bullet. As seen in Figure (38) the force exerted on the bullet increases rapidly with a smaller volume V_2 after loading, which would correspond to the insertion of gun powder. If this theory is valid the force curves in tensile test 9 should be lower than in 10 and 11 in Figure (25) where the volume is larger after loading without gun powder which they aren't. A difference is seen for the tensile test 12 and 13 in Figure (26) A and B respectively. The change of the tensile test curves after inserting a primer is not likely caused by plastic deformation in the neck of the case, stated by the fact that no contact on the neck of the case is made during the insertion in tensile test 12 and 13. This increase in force in test 12 and 13 could be explain by an under pressure but can't explain the increase seen comparing tensile test 6, 7 and 8 with 9, 10 and 11. This increase after the primer insertion could be one cause of the variation but the cause couldn't be explained through the scope of this thesis.

In tensile test 12 and 13 a decrease in frictional force compared to the other tensile test is seen after the initial maximum force. This is caused by the tapering at the bottom of the bullet Norma full metal jacket. The bottom of the bullet is a contributing variable to the increase in frictional forces. Variations due to plastic deformation seen in Figure (34) from the simulations is affected by the shape of the bottom part, which is explained further in the discussion.

6.3 SEM

As seen in Figure (27) there is a clear difference between the surfaces of the cases chosen for further evaluation. In A which is the case with the largest overall force. Transfer of material caused by adhesion can be seen as well as an even plastic deformation at the top of the neck of the case. This is suspected to be caused by that the central axis of the bullet and the case is in line. Large plastic deformation at the top of the case is also seen in B but suspected to be caused by an angle offset between the central axis of the bullet and the case during the loading procedure as the bullet is pressed into the case. This would explain the large extent of wear seen in the profilometer in the bottom of the bullet used with the case in Figure (30) B. The cases used with a bullet without cannelure in Figure (27) C and D show similar deformations on the surfaces. The wear mechanism can be seen caused by abrasive ploughing without adhesion. The wear depth is a bit larger on the case in C with the larger frictional force then in D.

For the bullet with the maximum frictional force A-C in Figure (28), many both deeper and more shallow grooves where material have been sheared of and adhered to the case in in Figure (27) A, the direction of which the material being transferred is due to loading or from the tensile test is circled in the figure. The bullet in figure D-F which had the largest frictional force for a bullet with a non-passivated surface shows a larger extent of abrasion and

adhesion. The force or shape of the curve isn't significantly different from the passivated although the damages is large. This is suspected to depend on the signs of the skew loading procedure, which deforms the neck of the case to a larger extent which decreases the pressure between the case and the bullet and different dominant wear mechanisms. The signs of the skew loading can be seen due to that the surfaces damages are more severe on one side of the bullet from the bottom to the cannelure, this will give a smaller real area of contact. This may explain why the force curves isn't higher for the non-passivated surface although the passivation has been shown to affect the wear and the force curves.

In Figure (28) G-I the bullet with the largest frictional force of the bullets without cannelure can be seen. It can be seen that there is more deformation on the surface due to ploughing on the bullet with the higher force compared to the bullet in Figure (28) J-L which had the lowest overall frictional force, this was also seen in the profilometer.

6.4 Profilometer

The profilometer pictures of the cases in Figure (29) A, B and C, D is very similar, transferred material due to adhesion can be seen on both. It can be seen that the wear depth is larger for the cases from tensile test 6 and 11 then for those in tensile test 1 and 2, explained by difference wear mechanism earlier due to increase in the diameter of the bullet. No significant difference is seen between the cases in E and F compared to G and H.

By comparing the bullets in Figure (30), the signs of the skew loading procedure can be seen in B where large damages have been made at the bottom of the bullet. The wear of the bullets is as also as seen in SEM much more severe for A, B and C, D then for E, F and G, H. The bullet in E and F shows more and deeper groves due to ploughing then the bullet in G, H, which explains the increased frictional force.

6.5 Hardness

The hardness of the cases is fairly constant except for the case with German material before the tool change, were the values are larger for those cases both with a measuring load of 1 Kilogram and 1 gram. The effect of increased hardness of the bulk material in the cases were tested further by varying the hardening parameter in the simulations.

The hardness of the bullets chosen for further examination showed very small variations. The surfaces of the bullets were damaged due to the tensile tests and the manufacturing which made it difficult to measure the hardness, why many values have been ignored and the last of the series an extra was made.

It can be noted that the surfaces of both the cases and the bullets have been strained hardened during manufacturing, loading and tensile tests, by comparing the results to Table (1) which shows the bulk hardness of the materials.

6.6 Simulations

As mentioned the goal of the simulations was to understand how different dimensions changed the shape of the force curve, maximum force and to find the areas with the largest stresses and contact pressure, therefore a simplified friction model was used with only a combined coefficient of friction (combined static and dynamic). As mentioned above the wear mechanism of the surfaces have a large impact to the size of the force and shape of the force curves.

The simulations in SM1 in Figure (31) shows the initial behavior seen in tensile test 1-3. The force drops to zero when the bottom of the bullet goes through the bottom of the neck due to the deformation from the loading. This do not correspond to the real tensile test in Figure (25) 1-3, where adhesion and abrasion is present which increases the friction force even with low pressure between the case and bullet. Therefore, a smaller diameter was used on the bottom of the case in SM2 where the stresses seen in Figure (37) B is largest. The behavior when the bottom of the bullet passed through could then be seen as in the real tensile tests. In the real tensile test, the contact between the bullets and the cases surface is different from the simulations as mentioned. It is therefore assumed to be the reason why both behavior from SM1 and SM2 and a larger force can be seen in the real tensile tests.

In SM3 when a larger diameter of the top of the bullet and a small tapering was used the shape of the beginning curve is close to the real tensile tests in Figure (25) 6-11. The increase of diameter will increase the pressure between the case and bullet why the initial force shows the peak as seen in Figure (25) 6-11. Because of the tapering of the bullet and the plastic deformation of the case seen in Figure (36), the force drops to zero rapidly. This is also as stated earlier that the real surfaces differ from the surfaces in the simulation models. The deformation on the bottom of the bullet as seen in Figure (34) causes a small increase of the force when it passes through the case. This is suspected to be one reason for increased forces, as a conclusion from both SEM pictures, profilometer pictures and the real tensile tests.

As seen in Figure (36) the displacement of the case in SM4 mainly is plastic, which was also seen in the measured real cases. As seen in Figure (24) the plastic deformation of the case made them equal or larger compared to the largest diameter of the bullet. In the simulation the same result was seen which means the hardening parameters used can be assumed to be valid.

To evaluate the effect of hardening on the frictional force the hardening parameter η was varied. The results in Table (11) shows that a smaller hardening parameter η of both the case and the bullet gave a larger frictional force. A smaller η corresponds referring to Section 3.3.2 to a material with higher strength. This means that cases with more cold work, short annealing time and high temperature will give a larger frictional force according to the model.

In SM4 the frictional force was larger with the thicker case compared to SM3. This would give a lower stress in the thicker case which corresponds to less plastic deformation. The displacement is connected to the plastic deformation, as seen the remaining plastic deformation in Table (12) is larger for SM3 then for SM4. In other words, the strength of the case is increased which gives decreases the stress and suppresses the plastic deformation, which would correspond the results with a smaller hardening parameter η.

6.7 Pressure inside the cartridge

As seen in Figure (38) the force exerted on the bullet due to pressure inside the cartridge increases rapidly for small volumes after the loading. If this force will be able to be exerted on the bullet in the opposite direction due to a under pressure compared to the atmospheric pressure, a complete seal and the potential overpressure that could build up during the loading have to be able to escape to pressurize to atmospheric pressure. The potential under pressure inside the cartridge would also increase the pressure between the neck of the case and the bullet. This theory can explain the behavior seen in Figure (26) but due to that the behavior is similar for tensile test 9-11, where 9 doesn't have gunpowder which means that the internal pressure would be smaller due to larger air volume to create the under pressure. More work has to be done to clarify further what causes the increase in force when the primer is inserted.

6.8 Press fit

The simplified elastic model shows that the thickness and the displacement mainly cause an increase in frictional force. The pressure is lower compared to the maximum values but comparable to the minimum values from the simulations. The maximum pressure values is assumed to be dependent on the tapered part between the chamber and neck of the case seen from Figure (37) B and that the hardening of the case due to plastic deformation affects the pressure. The shape and angle of the tapered part of the case could have a large impact on the frictional force.

7 Conclusion

The bullets and cases with the largest frictional forces that were investigated further both had transferred material from the bullet to the case due to adhesion. The abrasive wear mechanisms were changed from mainly ploughing with only little cutting for those with the smallest frictional forces, to mainly cutting for those with the highest frictional forces. A small increase in diameter on the bullet when the cannelure is pressed is found to be the cause of the change in wear mechanisms, responsible for increased frictional forces.

Even wear around the bullet and case was found to cause a large increase in frictional force. A close alignment between the central axis of the bullet and the central axis of the case during the loading procedure is assumed to cause the even wear. A skew alignment during the loading procedure in combination with a large area of the bottom of the bullet that plastically deforms the neck of the case to a larger extent, is assumed to cause the smallest frictional forces, variations and the larger plastic deformation in the neck for the non-passivated cases that was measured.

The insertion of the primer caused a changed in the measured force curves. This could partly be caused due to a under pressure inside the cartridge but can't be explained with certainty without further investigations. It is not likely caused by deformation of the neck when inserting and controlling the position of the primer.

The passivated layer caused smaller deformation of the neck during the loading procedure. The passivation is assumed to change the wear from dry to lubricated wear due to boundary lubrication. For bullets without cannelure the passivation layer gives more even force curves because abrasive ploughing is the preferred wear mechanism instead of cutting for the non-passivated. For bullets with a cannelure the passivation layer is penetrated in combination with the larger plastic deformation of the neck of the non-passivated cases no difference in frictional force is found.

The shape of the bullet was found to have the largest impact of the size and shape of the force curves. A small increase in the diameter caused a large increase in maximum force and a change in wear mechanisms. The bottom of the bullet plays a vital role in the size and shape of the force curve, where an increase of force was seen as the bottom of the bullet passed the point where the largest pressure was seen from the simulations. This behavior was not seen in tensile test 12 and 13 where the bullet was manufactured with a tapering. The cannelure deforms the neck of the case to a better fit around the bullets which is assumed to further increase the real area due to junction growth and therefore also the frictional force.

The transition between the chamber and the neck of the case is assumed have large impact of the size of the frictional force.

The loading procedure is assumed to have a large impact on the variations of the frictional force. To decrease variations the central axis of the bullet is suggested to be aligned with the central axis of the case.

8 References

[1] Katalog & Nedladdningsbart - Norma, https://www.norma.cc/sv/Om-Norma/Katalog-Nedladdningsbart/ (accessed 6 February 2018).

[2] 300 Win. Mag. - Norma, https://www.norma.cc/sv/Produkter/Jakt/300-Winchester- Magnum/ (accessed 17 May 2018).

[3] 308 Win - Norma, https://www.norma.cc/sv/Ammunitionsskolan/kaliberhistorik/.308-win/ (accessed 17 May 2018).

[4] Norma Line Up - Norma, https://www.norma.cc/sv/landing-page/sci-nr1-Norma-line-up/ (accessed 17 May 2018).

[5] Ivković B, Djurdjanović M, Stamenković D. The influence of the contact surface roughness on the static friction coefficient. 2000; 22: 41–44.

[6] Chowdhury M, Nuruzzaman DM, Mia AH, et al. Friction Coefficient of Different Material Pairs Under Different Normal Loads and Sliding Velocities. *Tribol Ind* 2012; 34: 18–23.

[7] Moshkovich A, Perfilyev V, Lapsker I, et al. Friction, wear and plastic deformation of Cu and α/β brass under lubrication conditions. *Wear* 2014; 320: 34–40.

[8] Hutchings IM. *Tribology: friction and wear of engineering materials*. Repr. Oxford: Butterworth-Heinemann, 2001.

[9] Stachowiak GW, Batchelor AW. *Engineering tribology*. Fourth edition. Oxford: Elsevier/Butterworth-Heinemann, 2014.

[10] Recent advances in separation of roughness, waviness and form - ScienceDirect, https://www.sciencedirect.com/science/article/pii/S0141635902001034 (accessed 6 February 2018).

[11] Askeland DR, Fulay PP, Wright WJ. *The science and engineering of materials*. 6th ed. Stamford, CT: Cengage Learning, 2011.

[12] The Brasses - Properties and Applications - Publication 117, http://copperalliance.org.uk/resource-library/pub-117---the-brasses (accessed 7 February 2018).

[13] Davis JR, ASM International (eds). *Copper and copper alloys*. Materials Park, OH: ASM International, 2001.

[14] Hertzberg RW, Vinci RP, Hertzberg JL. *Deformation and fracture mechanics of engineering materials*. Fifth edition. Hoboken, NJ: John Wiley & Sons, Inc, 2012.

[15] Dieter GE, Kuhn HA, Semiatin SL (eds). *Handbook of workability and process design*. Materials Park, OH: ASM International, 2003.

[16] Colgan M, Monaghan J. Deep drawing process: analysis and experiment. *J Mater Process Technol* 2003; 132: 35–41.

[17] Hajizadeh K, Tajally M, Emadoddin E, et al. Study of texture, anisotropy and formability of cartridge brass sheets. *J Alloys Compd* 2014; 588: 690–696.

[18] El-Danaf E, Kalidindi SR, Doherty RD. Influence of grain size and stacking-fault energy on deformation twinning in fcc metals. *Metall Mater Trans A* 1999; 30: 1223–1233.

[19] Yan H, Zhao X, Jia N, et al. Influence of Shear Banding on the Formation of Brass-type Textures in Polycrystalline fcc Metals with Low Stacking Fault Energy. *J Mater Sci Technol* 2014; 30: 408–416.

[20] Muhammed A, Abed A, Mustafa MA. Effects of recrystallization temperature on the mechanical properties of CuZn30 alloy. In: *2012 First National Conference for Engineering Sciences (FNCES 2012)*. 2012, pp. 1–6.

[21] Konkova T, Mironov S, Korznikov A, et al. Grain growth during annealing of cryogenically-rolled Cu–30Zn brass. *J Alloys Compd* 2016; 666: 170–177.

[22] Wiame F, Jasnot F-R, Światowska J, et al. Oxidation of α-brass: A photoelectron spectroscopy study. *Surf Sci* 2015; 641: 51–59.

[23] Lasky J. Ideal gas law. *Salem Press Encycl Sci*.

[24] Granta design limited, 'CES edupack,' Cambridge, 2016.

[25] Laddavdelningen - Norma, https://www.norma.cc/sv/Om-Norma/Foretagsinfo/var-personal/laddavdelningen/ (accessed 2 May 2018).

[26] Lundh H, 2000. *Grundläggande hållfasthetslära*. 1st ed. Stockholm: Instant Book AB.

9 Appendix A

Tensile test 1									Measurement of cases after tensile test			
Case	d (mm)	D (mm)	C (mm)	Weight (g)	Bullet	Db(mm)	Weight (g)	Fmax (kg)	Case	d (mm)	D (mm)	Kast (mm)
1	7,7925	8,4595	0,0231	13,97	9	7,823	11,028	9,91	1	7,8287	8,4941	0,0214
2	7,8003	8,4524	0,0103	14,095	45	7,823	11,033	11,6	2	7,8312	8,4948	0,0086
3	7,7939	8,4503	0,0377	14,001	77	7,824	11,036	12,4	3	7,8286	8,4892	0,0328
4	7,7967	8,4592	0,0165	14,045	64	7,823	11,042	9,82	4	7,8312	8,4936	0,0171
5	7,8092	8,4525	0,0158	14,017	62	7,824	11,034	9,65	5	7,8476	8,4972	0,0469
6	7,7962	8,4597	0,0226	14,071	29	7,824	11,034	11,1	6	7,8388	8,4913	0,0177
7	7,799	8,4569	0,0241	14,032	93	7,822	11,014	9,43	7	7,8376	8,4974	0,0176
8	7,7974	8,4571	0,0194	13,999	22	7,822	11,034	9,34	8	7,8372	8,4991	0,0199
9	7,7982	8,4601	0,0184	14,026	81	7,822	11,015	13	9	7,8294	8,4942	0,0211
10	7,7992	8,4593	0,0273	14,06	34	7,823	11,021	9,93	10	7,835	8,4938	0,0336
11	7,8026	8,458	0,019	14,043	94	7,822	11,04	10,5	11	7,8377	8,4939	0,0081
12	7,7958	8,4582	0,0145	13,976	43	7,824	11,051	9,96	12	7,8424	8,4933	0,0169
13	7,8009	8,4505	0,0201	14,019	13	7,824	11,037	10	13	7,8347	8,4961	0,0078

14	7,7985	8,4591	0,0099	14,082	20	7,824	11,031	9,62	14	7,8324	8,4954	0,0212
15	7,7944	8,4579	0,0182	14,045	54	7,823	11,045	13,5	15	7,8292	8,493	0,0061
16	7,8023	8,4522	0,003	14,093	58	7,822	11,027	7,32	16	7,8394	8,4983	0,0308
17	7,7986	8,4485	0,0295	14,002	21	7,824	11,038	10,9	17	7,8327	8,4945	0,0213
18	7,7996	8,4499	0,0142	14,035	28	7,823	11,017	11,7	18	7,8305	8,4931	0,0165
19	7,8025	8,4584	0,0216	14,09	44	7,823	11,035	9,24	19	7,8354	8,4968	0,0184

Tensile test 2									**Measurement of cases after tensile test**			
Case	d (mm)	D (mm)	C (mm)	Weight (g)	Bullet	Case	d (mm)	D (mm)	C (mm)	Weight (g)	Bullet	Case
1	7,8026	8,4543	0,0233	14,043	1	7,822	11,021	16,3	1	7,8506	8,4884	0,0303
2	7,7977	8,4539	0,0178	14,062	89	7,822	11,024	12,2	2	7,833	8,4842	0,0155
3	7,7988	8,4506	0,0092	14,089	88	7,823	11,044	14,7	3	7,8422	8,4853	0,0248
4	7,7974	8,4578	0,0179	14,045	12	7,822	11,018	18,8	4	7,8299	8,4873	0,0179
5	7,7996	8,4602	0,0105	13,995	48	7,824	11,034	12,3	5	7,8292	8,4918	0,0141
6	7,7941	8,4483	0,0247	13,997	56	7,824	11,047	13,9	6	7,8329	8,4875	0,0238
7	7,797	8,4582	0,0253	14,069	32	7,822	11,044	12,5	7	7,8342	8,4895	0,0253
8	7,7964	8,4551	0,0121	14,08	3	7,823	11,047	15,9	8	7,8277	8,4874	0,0122
9	7,7949	8,4528	0,0276	14,056	76	7,823	11,02	18,1	9	7,8346	8,4807	0,0246
10	7,7978	8,4587	0,0251	14,071	10	7,824	11,023	16	10	7,8297	8,4898	0,0214

11	7,7968	8,4543	0,012	14,087	52	7,824	11,022	17,6	11	7,8311	8,4849	0,01
12	7,7952	8,4532	0,0023	14,041	73	7,823	11,021	12,5	12	7,8355	8,4892	0,025
13	7,795	8,4533	0,0191	14,02	14	7,823	11,013	14,8	13	7,8413	8,4877	0,0365
14	7,7975	8,4525	0,0247	14,017	6	7,823	11,033	13,5	14	7,8339	8,4866	0,0219
15	7,7975	8,4547	0,0383	14,115	41	7,823	11,028	12,3	15	7,8307	8,4887	0,0361
16	7,7987	8,4566	0,0128	14,109	39	7,824	11,035	17,1	16	7,8327	8,4871	0,0036
17	7,7947	8,4541	0,0066	13,994	92	7,823	11,017	17,5	17	7,8308	8,4959	0,0096
18	7,7951	8,4538	0,0214	14,076	31	7,822	11,028	21,7	18	7,8308	8,494	0,0193
19	7,7951	8,4526	0,0077	14,03	35	7,824	11,031	13,7	19	7,8328	8,486	0,0149
20	7,7977	8,4578	0,0261	14,084	37	7,822	11,021	15,3	20	7,8275	8,4861	0,0294

Tensile test 6											**Measurement of cases after tensile test**			
Case	d (mm)	D (mm)	C (mm)	Weight (g)	Bullet	D11(mm)	D12(mm)	D13(mm)	Weight (g)	Fmax	Case	d (mm)	D (mm)	C (mm)
1	7,7942	8,46	0,0209	13,98	60	7,786	7,813	7,831	11,005	27,6	1	7,8574	8,5139	0,0178
2	7,8243	8,437	0,0141	14,02	12	7,782	7,811	7,831	11,02	26,1	2	7,8637	8,5292	0,0038
3	7,7991	8,46	0,0201	13,93	42	7,782	7,81	7,83	10,996	27	3	7,8533	8,5182	0,0213
4	7,7974	8,4607	0,0129	14,02	34	7,785	7,814	7,831	11,018	24	4	7,8472	8,5208	0,0144
5	7,8059	8,4594	0,0416	13,95	61	7,792	7,815	7,833	11,018	25	5	7,8587	8,5293	0,0116
6	7,7983	8,4625	0,014	13,97	55	7,808	7,818	7,834	11,005	28	6	7,8662	8,5192	0,0256
7	7,7967	8,4599	0,0277	14	21	7,789	7,816	7,832	10,999	26,6	7	7,8602	8,5231	0,0344
8	7,798	8,4635	0,0203	14,01	58	7,79	7,814	7,833	11,008	28,3	8	7,8494	8,5176	0,0198
9	7,7998	8,462	0,0248	13,99	36	7,79	7,812	7,831	11,022	28,7	9	7,853	8,5198	0,028
10	7,8013	8,4517	0,0099	14,03	26	7,785	7,812	7,832	10,999	28,1	10	7,8496	8,5166	0,0092

11	7,8018	8,4615	0,023	14,02	65	7,793	7,816	7,831	10,983	28,7	11	7,8486	8,5118	0,0181
12	7,7967	8,4612	0,0066	14,02	43	7,79	7,813	7,831	11,017	30,7	12	7,8544	8,5215	0,0099
13	7,797	8,4596	0,0181	14	63	7,791	7,814	7,83	10,998	27,5	13	7,8601	8,5323	0,0315
14	7,7961	8,4638	0,0117	14,01	69	7,782	7,815	7,832	11,013	33,9	14	7,8347	8,5154	0,0373
15	7,7981	8,4637	0,0183	14	15	7,785	7,816	7,833	11,016	27,1	15	7,8526	8,5211	0,0156
16	7,7965	8,4599	0,0136	13,97	18	7,786	7,814	7,831	10,986	22,4	16	7,8439	8,5202	0,0041
17	7,7983	8,4625	0,0302	14,06	67	7,797	7,812	7,832	11,009	26,3	17	7,8555	8,5246	0,0326
18	7,7967	8,459	0,0206	14,02	62	7,787	7,81	7,832	11,007	24,3	18	7,8482	8,5162	0,0137
19	7,7987	8,4615	0,0156	13,96	32	7,78	7,811	7,832	11,015	32,3	19	7,8407	8,5115	0,0109
20	7,8014	8,4595	0,0069	13,97	10	7,788	7,815	7,833	11,009	26,8	20	7,8547	8,5246	0,0084

10 Appendix B

Date	2018-02-13			2018-02-15			2018-02-16		
Material Origin	Switzerland			Germany			Germany		
Tool change	Before			Before			After		
Case	1 mm	3 mm	6 mm	1 mm	3 mm	6 mm	1 mm	3 mm	6 mm
1	105	107,4	114	108,6	111	120,2	102	106,4	114
2	106,6	110	114,6	107,6	110,2	116,8	103	106	114,2
3	103,6	106,6	115,6	106,2	112	119,2	104	107,8	115
4	106,2	110,8	118	108,6	113,2	117,2	103,2	106,2	116,2
5	105,6	107,8	115	107,6	112,4	117,8	104,6	106,2	114,6
Average	105,4	108,52	115,44	107,72	111,76	118,24	103,36	106,52	114,8

Bullet	A		B		C		D		
Series	1	2	1	2	1	2	1	2	3
1	164	151	159	158	168	160	147	128	144
2	153	151			142	152	163	169	155
3		164	158	153	154	159	154	155	151
4	153	159	158	167	158	153	163	168	158
5	167	167	159		159	150	171		148
6	136	151	159	158	149	175	157	153	148
7	158	122	150	160	159	150	151	175	152
8	161	158	146	172		151	143		146
9		168		144			149	157	144
10	162	153	154	148	155			144	141
Average	157	154	155	157	155	156	155	156	148
	155		156		156		156		